

Contents lists available at ScienceDirect

# European Journal of Medicinal Chemistry

journal homepage: www.elsevier.com/locate/ejmech



# Research paper



# Synthesis and biological characterization of an orally bioavailable lactate dehydrogenase-A inhibitor against pancreatic cancer

Horrick Sharma <sup>a,\*</sup>, Somrita Mondal <sup>a</sup>, Uzziah Urquiza <sup>b</sup>, Colter Esparza <sup>b</sup>, Seth Bartlett <sup>a</sup>, Landon Santa-Pinter <sup>a</sup>, Hanna Hill <sup>b</sup>, Madalyn White <sup>b</sup>, Pragya Sharma <sup>b</sup>, Lerin Luckett-Chastain <sup>c</sup>, Anne Cooper <sup>d</sup>, Mohammad Rasel <sup>d</sup>, Philip Gao <sup>e</sup>, Kevin P. Battaile <sup>f</sup>, Surendra K. Shukla <sup>g</sup>, Scott Lovell <sup>d</sup>, Michael A. Ihnat <sup>c</sup>

# ARTICLEINFO

Handling Editor: Dr. Z Liu

Keywords:
Lactate Dehydrogenase-A Pancreatic cancer
Small molecule inhibitor
Lactate
Pharmacokinetics
OXPHOS

# ABSTRACT

Lactate dehydrogenase-A (LDHA) is the major isoform of lactate dehydrogenases (LDH) that is overexpressed and linked to poor survival in pancreatic ductal adenocarcinoma (PDAC). Despite some progress, current LDH inhibitors have poor structural and physicochemical properties or exhibit unfavorable pharmacokinetics that have hampered their development. The present study reports the synthesis and biological evaluation of a novel class of LDHA inhibitors comprising a succinic acid monoamide motif. Compounds 6 and 21 are structurally related analogs that demonstrated potent inhibition of LDHA with IC50 of 46 nM and 72 nM, respectively. We solved cocrystal structures of compound 21-bound to LDHA that showed that the compound binds to a distinct allosteric site between the two subunits of the LDHA terramer. Inhibition of LDHA correlated with reduced lactate production and reduction of glycolysis in MIA PaCa-2 pancreatic cancer cells. The lead compounds inhibit the proliferation of human pancreatic cancer cell lines and patient-derived 3D organoids and exhibit a synergistic cytotoxic effect with the OXPHOS inhibitor phenformin. Unlike current LDHA inhibitors, 6 and 21 have appropriate pharmacokinetics and ligand efficiency metrics, exhibit up to 73% oral bioavailability, and a cumulative half-life greater than 4 h in mice.

# 1. Introduction

Cancer cells differ from normal cells by upregulating glycolysis and glucose uptake and converting pyruvate to lactate even in the presence of oxygen (Warburg effect) [1]. Despite having functional mitochondria, cancer cells reprogram their metabolism from oxidative phosphorylation (OXPHOS) to aerobic glycolysis for survival and growth [2]. Lactate dehydrogenases (LDH) mediate the Warburg effect and convert pyruvate to lactate, simultaneously producing NAD+, which drives glycolysis for ATP production [3]. Further, the pyruvate phosphate pathway and hexosamine biosynthesis provide cancer cells with the biomass and cellular building blocks, amino acids, nucleotides, and lipids needed for cancer cell proliferation [4,5]. The glycolytic rate of cancer cells is about 30 folds higher than in normal cells, compensating for the low turnover of ATP from glycolysis compared to the ATP produced from OXPHOS [6–8]. KRAS mutations upregulate glucose transporter-1 and overexpress glycolytic enzymes, including LDHA, in pancreatic adenocarcinoma (PDAC)

[9,10]. Increased LDHA and the resulting lactic acid are associated with poor overall survival in PDAC patients [11,12]. The elevated lactate in the tumor microenvironment favors tumor promotion, metastasis, and immune escape [13–17]. Silencing of LDHA resulted in reduced pancreatic tumor growth in a mouse xenograft model [18]. Further, induced knockout of LDHA in a genetically engineered mouse model of non-small-cell lung cancer inhibits tumorigenesis and progression of established tumors without serious systemic toxicity [19]. In contrast, silencing LDH-B had no apparent effect on tumor cell survival [20]. Compelling evidence supports the development of LDHA inhibitors that may improve resistance to current chemotherapy and immunotherapy and offer novel therapeutic options for cancer treatment [21,22]. Some promising LDHA/B small molecule inhibitors (Fig. 1) include GSK2837808A [23], GNE-140 [24], FX-11, [25] NCATS-SM1441 [26], NCATS-SM1440 [26], and compound 1 [19]. FX-11 was a lead LDHA inhibitor discovered a decade ago that demonstrated inhibition of human pancreatic cancer xenografts. However, its development was halted as it showed

<sup>&</sup>lt;sup>a</sup> Department of Pharmaceutical Sciences, College of Pharmacy, Southwestern Oklahoma State University, Weatherford, OK, USA <sup>b</sup> Department of Biological & Biomedical Sciences, Southwestern Oklahoma State University, Weatherford, OK, USA

<sup>&</sup>lt;sup>c</sup> Department of Pharmaceutical Sciences, College of Pharmacy, University of Oklahoma Health Sciences Center, Oklahoma City, USA <sup>d</sup> Protein Structure and X-ray Crystallography Laboratory, The University of Kansas, Lawrence, KS, USA <sup>e</sup> Protein Production Group, The University of Kansas, Lawrence, KS, USA <sup>e</sup> New York Structural Biology Center, Upton, NY, USA <sup>e</sup> Department of Oncology Science, OU College of Medicine, Oklahoma City, USA

nonspecific cytotoxicity due to its catechol and formation of the *o*-quinone metabolite [25,27]. Subsequent efforts have led to the identification of potent LDH inhibitors, but they did not exhibit properties of a drug-like lead. GSK2837808A and GNE-140 failed to show efficacy because of poor pharmacokinetics and rapid clearance *in vivo* [23,28]. NCATS-SM1440 and NCATS-SM1441 are pyrazole-based LDH inhibitors that showed that inhibition of LDHA *in vivo* reduced the growth of glycolytic tumors. However, NCATS-SM1440 and NCATS-SM1441 required intravenous administration and have undesirable physicochemical properties, being highly lipophilic with large molecular weights [26,29]. Compound 1 is reported to have modest inhibition of MiaPaCa-2 xenograft growth, but its pharmacokinetics was not shown. There is an unmet need to find novel scaffolds and lead compounds with druglike properties, which could be developed as clinical candidates to target lactate production for cancer therapy [26].

### 2. Results and discussion

In our previous study, we conducted virtual screening and identified several novel hits against LDHA [30]. In this work, we report the synthesis, SAR, structural and biological characterization, and pharmacokinetic evaluation of succinic acid monoamide scaffold (Fig. 2), which led to the identification of two related compounds, 6 (an ester analog) and compound 21 (carboxylic acid derivative), as orally available LDHA inhibitors that inhibit the proliferation of pancreatic cancer cell lines and 3D pancreatic cancer organoids.

### 2.1. Synthesis

The synthesis of compounds containing a succinic acid monoamide moiety or their derivatives is shown in Scheme 1. First, substituted phenylacetic acid starting materials were converted to their corresponding methyl esters, intermediate II. The next step involved a nucleophilic substitution reaction with

tert-butyl bromoacetate to give diester derivatives III. Selective hydrolysis of the tert-butyl esters was achieved using trifluoroacetic acid (TFA) to yield corresponding acid- containing intermediates IV. In the next amide coupling reaction, the acid intermediates (4a-4f) were reacted with diverse amines to give ester analogs (compounds 5–18). The final step involves hydrolysis of the methyl esters to give acid-containing analogs 20–28.

The synthesis of compounds **33–36** is shown in Scheme 2 *p*-chlorobenzaldehyde was reacted with malonic acid and ammonium nitrate using the Rodionow–Johnson reaction to give the  $\beta$ -aryl- $\beta$ -amino acid, intermediate **30**. In the next step, the acid was converted to ethyl ester analog **31**, which was reacted with acid chlorides to give corresponding amide intermediates **32a-32d**. Finally, the ethyl esters were hydrolyzed to afford target compounds **33–36**. *2.2. Separation and characterization of isomers of 21* 

Compounds represented by general structures **V** and **VI** (Scheme 1) contain a chiral center, and synthesis was expected to form a racemic mixture. Further, we suspected hindered rotation about the amide bond and formation of *syn*-and *anti*-atropisomers in the amide coupling step. This was evident from the peaks observed on LCMS (supplementary information, Fig. S1). To obtain and characterize pure isomers of **21**, we separated the *syn*- and *anti*-atropisomers, fractions A1 and A2, by prep HPLC, followed by separation of the (*R*)- and (*S*)-enantiomers by chiral chromatography (Fig. S1). The purity of separated isomers is shown in Fig. S2. Next, we successfully prepared the single crystals of A1P1 and A1P2 isomers of **21**. The structural analysis was carried out through single crystal X-ray diffraction. A1P1 and A1P2 isomers crystallize in non-centrosymmetric space group *P2*<sub>1</sub>. The crystal structure and crystallographic data at 100 K are shown in Fig. 3 and Supporting Information Table S1, respectively. The compound crystallizes in the monoclinic P space group P21. Both compounds with the same chiral

Fig. 1. Chemical structures of known Lactate Dehydrogenase inhibitors.

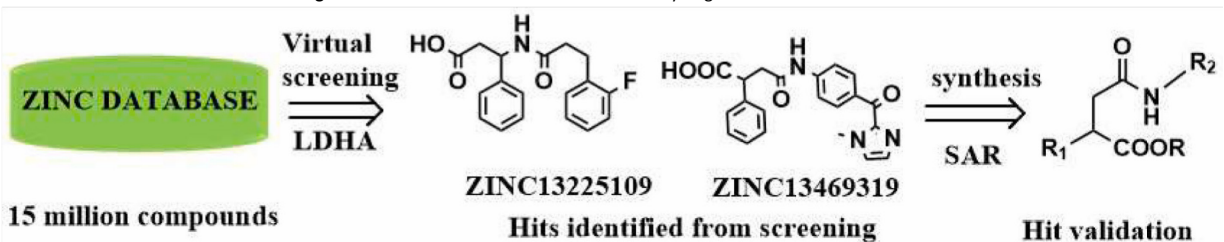


Fig. 2. Rational design of succinic acid monoamide derivatives as novel LDHA inhibitors.

Scheme 1. (a) MeOH, H<sub>2</sub>SO<sub>4</sub>, rt, 2 h, 84.2%–90.1% yield; (b) BuLi, diisopropyl amine, THF, *tert*-butyl bromoacetate, – 78 °C- rt, 6 h, 45.9%–89.5% yield; (c) TFA, DCM, rt, 4 h, 62.8% - quantitative yield; (d) method A: Oxalyl chloride, DMF, DCM 0°C-rt, 2 h, then R<sub>2</sub>NH<sub>2</sub>, Et<sub>3</sub>N, DCM, rt, overnight; Method B: HATU, Et<sub>3</sub>N R<sub>2</sub>NH<sub>2</sub>, DCM, 24 h–72 h, 24.2%–90.7% yield; (e) LiOH, H<sub>2</sub>O, THF, rt, 3 h, 22.9%–74.3%.

Scheme 2. (a) Malonic acid, ammonium nitrate, methanol, reflux, overnight, 47.9% yield; (b) Thionyl chloride, ethanol, 65 °C, 6 h, 81.3% yield; (c) Acid chloride, pyridine, THF, DMF, rt, 24 h or (method B) Acid, HATU, Et<sub>3</sub>N, DCM, rt, 24 h, 66.07%–93.4%; (d) LiOH, H<sub>2</sub>O, THF, rt, 3 h, 10.8%–49.7%.

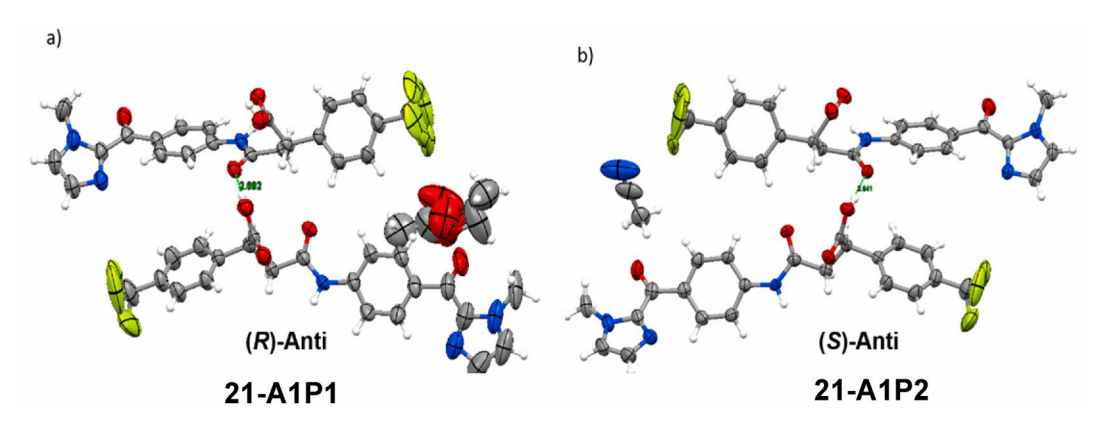


Fig. 3. Crystal structure of compound 21-A1P1 (a) and 21-A1P2 (b). Color code: C, gray; N, blue; O, red; H, white and F, light green.

space group were always obtained. A1P1 and A1P2 both show the same *anti-*amide conformation, and the absolute configuration was determined as the *R-anti* for A1P1 and *S-anti* for A1P2, respectively. Two crystallographically independent molecules exist for both compounds, with one crystalized solvent molecule in the pore (ethyl acetate for A1P1 and acetonitrile for A1P2). The inter-hydrogen bond is formed between the carboxyl group and the oxygen atom of the amide group of two neighboring molecules. The fractions A2-P1 and A2-P2 could not be crystalized despite several attempts, and we hypothesize that these may have the amide group in the *syn* conformation. The four isomers demonstrated similar inhibition of LDHA (Supporting Information, Fig. S3), and thus, we used the racemic mixture for subsequent studies.

# 2.3. Structure-activity relationship (SAR)

The compounds for SAR are represented by general structures "VII" and "VIII" in Fig. 4. The "R" group in the structure VII is either a methyl or hydrogen, representing a methyl ester or its corresponding carboxylic

Fig. 4. General compounds for SAR. 
$$R_1$$
  $R_2$   $R_2$   $R_2$   $R_3$   $R_4$   $R_4$   $R_5$   $R_5$   $R_5$   $R_6$   $R_7$   $R_8$   $R_1$   $R_1$   $R_1$   $R_1$   $R_1$   $R_2$   $R_3$   $R_4$   $R_5$   $R_5$   $R_6$   $R_7$   $R_8$   $R_1$   $R_1$   $R_1$   $R_1$   $R_2$   $R_3$   $R_4$   $R_5$   $R_5$   $R_5$   $R_6$   $R_7$   $R_8$   $R_1$   $R_1$   $R_1$   $R_2$   $R_2$   $R_3$   $R_4$   $R_1$   $R_1$   $R_2$   $R_3$   $R_4$   $R_5$   $R_6$   $R_8$   $R_8$   $R_8$   $R_8$   $R_9$   $R_9$ 

20-28 containing a carboxylic acid were characterized in biochemical LDHA/B assays. An ester analog, with an unsubstituted phenyl ring at the R<sub>1</sub> position and a N-methyl-1H-imidazole -2-phenone moiety at the R<sub>2</sub> position, compound 18, showed (Table 1) low micromolar inhibition of LDHA, with an IC<sub>50</sub> of 2.4 µM. Substitution of the phenyl ring at the para-position remarkably affected the LDHA inhibitory potency. For example, substituting a fluoro group in compound 19 resulted in the loss of potency with IC<sub>50</sub> value of 33.6 μM. Similarly, a significant drop in potency was observed when an electron-donating methoxy group was substituted at the para-position in compound 17 (IC<sub>50</sub> value of 50 μM). The substitution of a lipophilic halogen improved activity. For example, a 4-chloro moiety in compound 5 exhibits improved potency to sub-micromolar levels (IC<sub>50</sub> = 0.181 μM). A more lipophilic trifluoromethyl group in compound 6 resulted in a significant gain in potency inhibiting LDHA with IC<sub>50</sub> of 43 nM. The increase in potency could be understood from the crystal structure of compound 21 in complex with LDHA, discussed in more detail in the subsequent section. Notably, the trifluoromethyl group of 21 makes van der Waals interaction and occupies a pocket formed by lipophilic residues Val208, Gly207, and Gly202 at the interface of LDHA chains A and D. Compound 28, containing a bicyclic ring system, showed moderate inhibition of LDHA, suggesting that a bulkier substituent at the  $R_1$  position may not be optimal. With respect to the 'R" group, both methyl esters and carboxylic acid retained activity. The methyl esters were generally more potent than the corresponding carboxylic acid analogs. However, the difference may not be substantial in some instances. For example, compound 6 (LDHA IC<sub>50</sub> = 43.7 nM) and compound 21 (LDHA IC<sub>50</sub> = 72 nM) retained appreciable activity. Unlike many reported LDHA inhibitors, which possess carboxylic acid (Fig. 1), the acidic group is not absolutely required for activity in this series of compounds. This observation is supported by the co-crystal structures of compound 21, which do not show any charged cationic amino acid present near the carboxylic acid for ionic interactions. Instead, the residues observed are polar, uncharged amino acids that can exhibit H-bonding interactions with both the acid and the ester. The SAR at the R2 position (Structure VII, Fig. 4) significantly affected potency. Several compounds (7-16) and (22–26) with diverse R<sub>2</sub> substituents were synthesized. Compound 8 with a single heteroaromatic ring system was inactive with  $IC_{50} > 100 \mu M$ . Compounds with two aromatic rings retained activity. In particular, the N-methyl-1H-imidazole in potent analogs 6 and 21 and other active analogs 5 and 20 suggests it could be essential for activity. The cocrystal structure showed that the N-methyl imidazole ring of 21 makes a critical pi-stacking interaction with the pyrrolidine ring of Pro215. Substitution of N-methyl imidazole by a phenyl or indole ring in 9 and 13 resulted in a drop in potency. Further, the SAR showed that the ketone linker between the two aromatic rings could be crucial. This is explained by the drop or loss of activity in compounds (7, 11, 12, 14, and 15) in which the two aromatic rings are directly connected. Replacing ketone with a methylene linker in compound 10 also resulted in activity loss (LDHA IC<sub>50</sub> = 100  $\mu$ M). Next, to ascertain if the core structure VII, representing a salicylic acid monoamide, is essential for activity, we synthesized compounds 33-36. The structural changes (Fig. 4) include a reverse amide moiety, and the  $R_{\mbox{\scriptsize 1}}$  substitution is attached to the adjacent carbon in Structure VIII. As seen in Table 1, compounds 33-36 were inactive

Compound	Structure	LDHA IC <sub>50</sub> ± standard deviation (SD) (μM) <sup>a</sup>	LDHB IC <sub>50</sub> $\pm$ standard deviation (SD) ( $\mu$ M) <sup>a</sup>
5	CI COOCH,	$0.181 \pm 0.029$	$26.49 \pm 6.64$
6	P <sub>SC</sub> COOCH <sub>3</sub>	$0.0437 \pm 0.006$	$15.48\pm4.83$
7	F <sub>3</sub> C - NO COOCH <sub>3</sub> - NO	$71.50 \pm 8.15$	$60.63 \pm 16.32$
8	COOCH3	>100	>100
9	F <sub>3</sub> CC COOCH <sub>3</sub>	$15.72\pm5.39$	$52.74 \pm 7.86$
10	F <sub>2</sub> C-CH <sub>3</sub> N-N COOCH <sub>3</sub> N-N	$100.63 \pm 2.83$	52.74 ± 7.86
11	F <sub>3</sub> C OOCH <sub>3</sub>	>100	>100
12	F <sub>3</sub> C - HN - S	>100	>100
13	F,COOCH,	$22.32 \pm 4.32$	$\textbf{40.24} \pm \textbf{4.26}$
14	Social So	$62.58 \pm 15.68$	$39.52 \pm 5.46$
15	ON NOT COOCH <sub>3</sub>	$66.40 \pm 1.43$	$43.23 \pm 5.43$
16	CHOCH <sub>3</sub>	$26.85\pm2.07$	$25.48 \pm 6.77$
17	Neo Cooch,	$50.05\pm0.28$	$38.90 \pm 4.06$
18	OCCH,	$2.49\pm0.19$	$58.33 \pm 2.71$
19	Q N N N N N N N N N N N N N N N N N N N	$37.76 \pm 8.38$	$43.26 \pm 11.43$
20	CI COOH	$0.19\pm0.08$	$58.36\pm3.04$
21	F <sub>S</sub> C COOH	$0.072\pm0.01$	$1.2\pm0.32$
22	F <sub>3</sub> C-\(\bigc\)-\(\bigc\)-\(\bigc\)-\(\bigc\)-\(\bigc\)-\(\bigc\)-\(\bigc\)-\(\bigc\)	>100	>100

(continued on next page)

**Table 1**Biochemical IC<sub>50</sub> values of compounds against LDHA and LDHB.

Table 1 (continued)

Compound	Structure	LDHA IC $_{50}$ $\pm$ standard deviation (SD) $(\mu M)^a$	LDHB IC <sub>50</sub> $\pm$ standard deviation (SD) $(\mu M)^a$
23	P <sub>3</sub> CCOOH	$79.3 \pm 14.65$	$72.48 \pm 3.01$
24	F <sub>3</sub> C — HN — S	>100	>100
25	N-N N N N N	$39.43 \pm 15.68$	$33.04 \pm 6.75$
26	F <sub>2</sub> C COOH	>100	>100
27	Neo COOH	$54.48 \pm 2.34$	$\textbf{42.24} \pm 3.36$
28	O-N-COOH	$29.91 \pm 9.92$	$38.12\pm1.39$
33	COOH COOH	>100	>100
34	COOH	>100	>100
35	CLI N COOH	>100	>100
36	F <sub>3</sub> C ССССССОН	>100	>100

 $<sup>^{\</sup>rm a}$  The assays were performed in triplicates and the data is presented as mean  $\pm$  SD (n = 3).

(LDHA IC<sub>50</sub> > 100  $\mu$ M), implying the R<sub>1</sub> substituent adjacent to the carboxylic acid/ester group could be essential for activity. The LDHA inhibition doseresponse curve for the two most potent compounds, **6** and **21**, is shown in Fig. 5.

We also characterized compounds against LDHB. In general, compounds were selective for LDHA, with compound 6 being 350-fold more

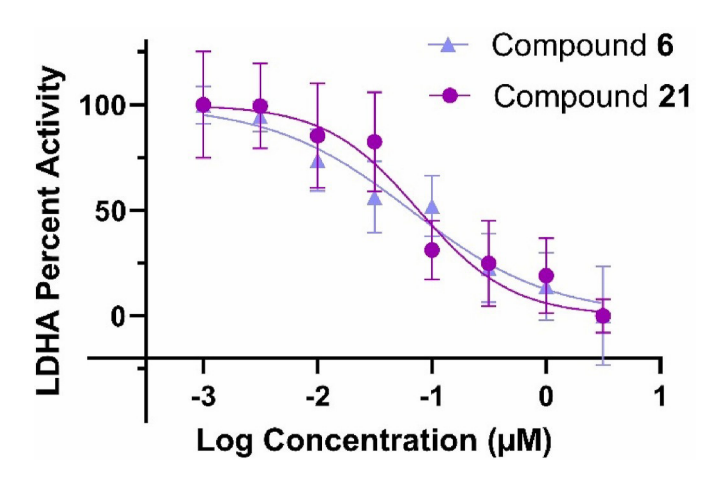


Fig. 5. Compounds 6 and 21 LDHA dose-response curves. Data are shown as mean  $\pm$  SD from n = 3, three technical and three biological replicates.

potent for LDHA. Analysis of TCGA and GTEx RNA sequencing data from Gene Expression Profiling Interactive database show that LDHA is overexpressed in most tumors, including PDAC. In contrast, LDHB showed reduced expression in pancreatic adenocarcinoma compared to their adjacent noncancerous pancreatic tissue counterparts. Compound **21** inhibits LDHA and LDHB with 16-fold greater selectivity for LDHA. The structural basis of selectivity for LDHA is likely due to their binding to an allosteric site on LDHA, which is discussed in the following section on the X-ray co-crystal structure of LDHA and **21**.

# 2.4. Binding affinity by SPR

We determined the affinity (measure of the strength of binding) and kinetics (speed of association and dissociation) of compound  $\bf 6$  binding to LDHA using surface plasmon resonance (SPR). SPR measures the interaction between molecules in real time, in this case, by immobilizing the LDHA protein to the sensor chip surface and injecting a range of compound concentrations over the chip. The binding of compound to the protein generates a response (RU) that is proportional to the bound mass by measuring a change in the refractive index at the chip surface. The affinity constant ( $K_D$ ) was determined by kinetic fitting of the association and dissociation (on- and off-rate) signals or by plotting the level of steady-state binding for each concentration (equilibrium fitting) (Fig. S4). The kinetics was determined using the 1:1 Langmuir model.

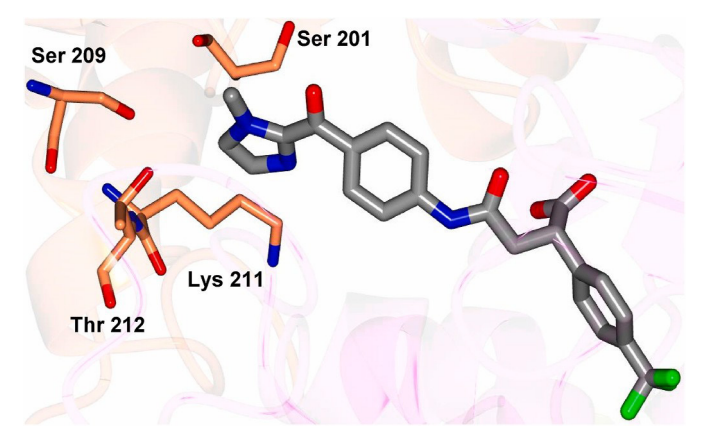
Compound 6 binds to LDHA with a fast association rate ( $K_{on}$  of 1.17 × 105 M<sup>-1</sup>s<sup>-1</sup> <sup>1</sup>) and showed a dissociation  $K_{\rm off}$  of 1.68 × 10<sup>-3</sup> s<sup>-1</sup>, though the kinetic constants could not be uniquely determined. The kinetic parameters may be approximate if the sensogram does not show sufficient curvature during the dissociation phase. However, for compound 6, the kinetic KD of 14.5 nM aligned more closely with the observed biochemical IC<sub>50</sub> value of 44 nM for LDHA. Molecules with a fast on-rate have a much higher tendency to rebind to the receptor after dissociation, may show improved in vivo efficacy, and are advantageous since a low dose may be required and may help if the bioavailability of the drug is low. Slower dissociation rates may be essential to extend the duration of action, particularly if the compound has rapid clearance. The compound binds with greater affinity in the presence of NADH ( $K_D$  = 14.5 nM) than in the absence of NADH ( $K_D$  = 132 nM). For steady-state requirement, the sensorgrams must reach a steady state during sample injection, i.e., the compound should show a stable binding level at the time point used for calculation before the end of the injection and the compound's subsequent dissociation. As expected, the steady-state binding affinity was significantly more potent ( $K_D = 523 \text{ nM}$ ) in the presence of NAHD than in the absence of NADH ( $K_D = 52.2 \mu M$ ).

# 2.5. X-ray co-crystal structure of LDHA and 21

To understand molecular interactions and ascertain the binding modes of our compounds, we solved two crystal structures of LDHA complexed with compound **21**. LDHA-21-monoclinic (m) structure adopts a tetramer quaternary structure, and inhibitor **21** is positioned between two subunits (A and D) directed toward the surface, as shown in Fig. 6A. Prominent electron density consistent with the *S*-enantiomer of the inhibitor was observed (Fig. 6B), and hydrogen bond interactions are formed with the side chain –OH groups of Thr212 in both subunits and the backbone carbonyl of Gly202 in subunit B. (Fig. 6C). Residues near the inhibitor include Thr209, Asn204, Lys211, and Pro215 of subunit A, as well as Asn204 and Ser209 of subunit D. Compound **21**, is positioned within a pocket formed by mostly uncharged residues, as shown in Fig. 6D.

Although no direct contacts are formed, the methyl-imidazole ring of **21**, which is directed towards the surface, is in proximity ( $^{\sim}3.5$  Å - 4.0 Å) to LDHA residues Ser201, Ser209, Lys211, and Thr212 related by crystallographic symmetry (Fig. 7).

The LDHA-21-m structure is similar to previously determined LDHA structures, such as the NADH bound complex (PDB 5ZJD), which yielded



compound **21** bound structure adopts the closed, active conformation in each subunit (Fig. S5C). Binding to an allosteric site could be a reason for the selectivity for LDHA over LDHB. The selectivity for LDHA was also observed for the allosteric LDHA inhibitor machilin A [31]. This is unlike LDH inhibitor **GNE-140**, which inhibits LDHA and LDHB and occupies the catalytic site occupied by pyruvate close to NADH [32].

The other crystal structure belongs to the orthorhombic *P* form and is similar to the LDHA-**21**-m structure overall. However, electron density for the inhibitor was observed near the NADH binding site and was best modeled with the *R*-enantiomer (Fig. 8A). No electron density was present in the ligand binding site that was observed for the LDHA-**21**-m structure. The inhibitor forms hydrogen bond contacts with Lys80, Tyr82, Asn83, and Tyr126. The trifluoromethyl aryl group of the inhibitor is directed towards the surface and is positioned in a groove formed by Tyr09, Leu279, Lys277, and Leu302 of symmetry-related LDHA subunits (Fig. 8B). The methyl-imidazole ring is present

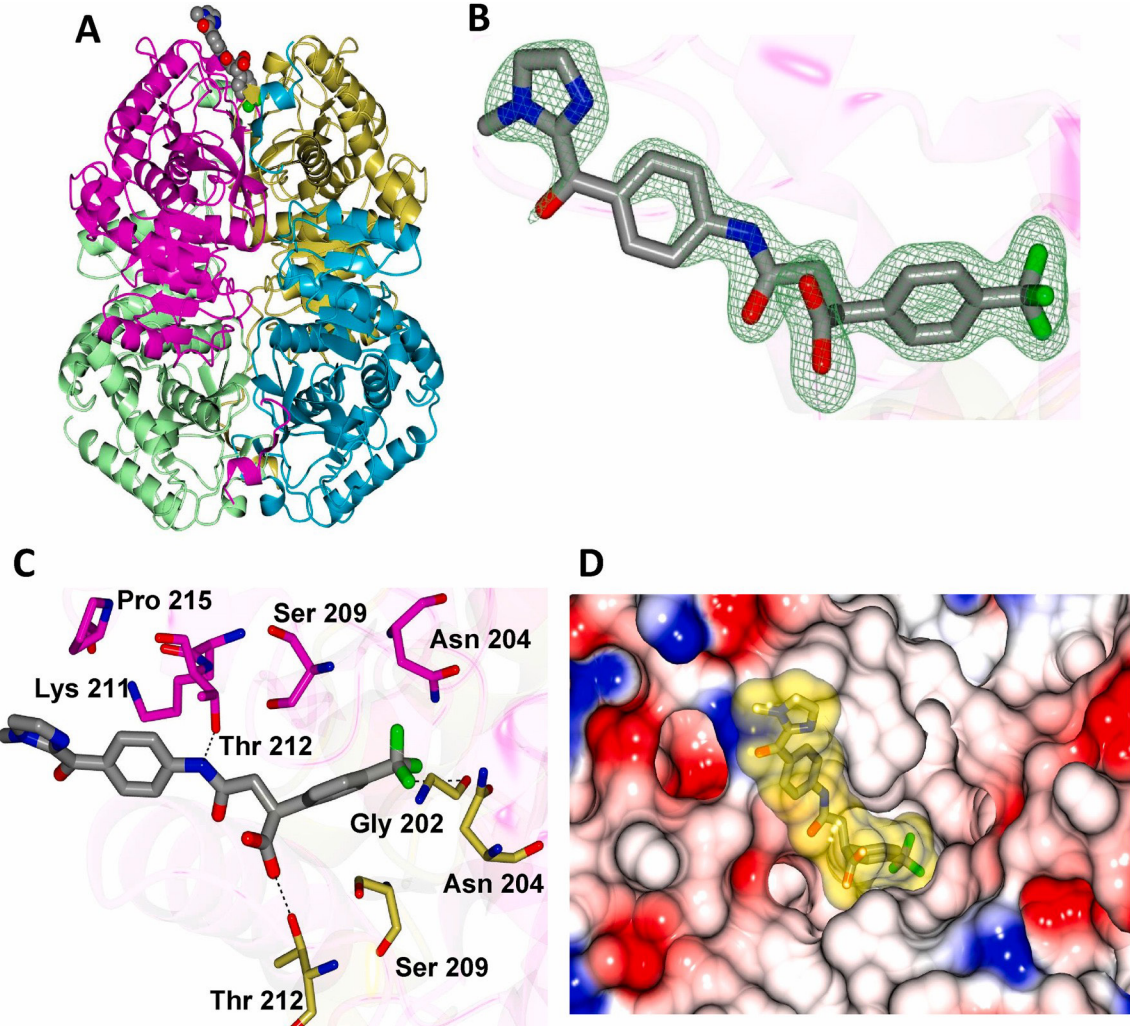


Fig. 6. Structure of the LDHA complex with compound 21. (A) LDHA tetramer colored magenta (subunit A), cyan (subunit B), green (subunit C) and gold (subunit D). The inhibitor, 21, is rendered at spheres. (B) Electron density (Fo-Fc) omit map (green mesh) contoured at 3σ for the inhibitor. (C) Hydrogen contacts (dashed lines) between LDI56 and subunits A and D. (D) Electrostatic surface rendering showing the binding mode of 21 (cylinders and yellow surface) to LDHA.

**Fig. 7.** Orientation of the methyl-imidazole ring of compound **21** near LDHA residues in the region occupied by the adenine ring of NADH (Fig. 8C). related by crystallographic symmetry (coral).

an RMSD deviation of 0.48 Å between  $C\alpha$  atoms (328 residues aligned). Notably, compound 21 binding site is approximately 25 Å from the NADH binding site (supplementary information, Fig. S5A). The inhibitor occupies a similar binding site observed for the structure with the natural product inhibitor machilin A (Fig. S5B) [31]. It was noted that machilin A binds to the "open" conformation of LDHA in the NADH binding site loop spanning Ala97 to Leu108 which produced inactivated form. Interestingly, this loop in the

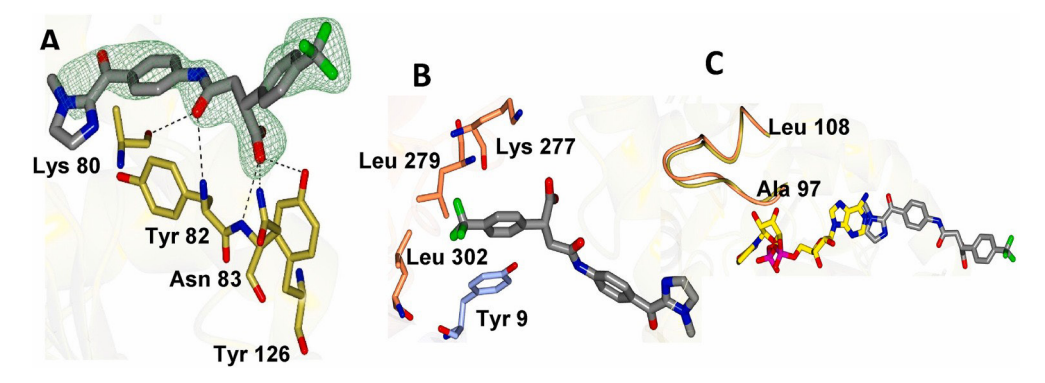


Fig. 8. Structure of the LDHA-compound 21-o complex. (A) Electron density (Fo-Fc) omit map (green mesh) contoured at 3σ for the inhibitor and hydrogen bonds (dashed lines) between 21 and subunit D. (B) Orientation of compound 21 trifluoromethyl aryl ring near LDHA residues related by crystallographic symmetry (coral and light blue). (C) Superposition of LDHA complexed with 21 (gray) with the NADH bound structure (PDB 5ZJD).

2.6. Compound **21** reduces lactate secretion and intracellular lactate levels

Elevated lactate in the tumor microenvironment is involved in carcinogenesis, which favors tumor promotion, metastasis, and immune escape. To characterize the effect of 21 on lactate levels, we determined the lactate secreted by MIA PaCa-2 cells after 6 h (h) of compound treatment. MIA PaCa-2 cells were treated with 21 (15  $\mu\text{M}$  and 30  $\mu\text{M}$ ), and the lactate secreted in the culture medium after 6 h was determined using a colorimetric/fluorometric lactate assay kit. The assay was performed with cells cultured in varied nutrient conditions: regular DMEM medium (25 mM glucose, 2 mM glutamine, and 1 mM pyruvate) and in nutrient-stressful conditions with low glucose (10 mM) and no pyruvate in the cell culture media. In either condition, 21 caused a significant reduction (Fig. 9A and B) in lactate secreted in the extracellular medium in a dose-dependent manner.

Next, we determined the changes in the intracellular levels of lactate, pyruvate, and citric acid cycle metabolites induced by treatment of 21 in MIA PaCa-2 cells. We treated MIA PaCa-2 cells with  $15~\mu M$  concentration of compound 21 for 6~h and 24~h and the concentration of intracellular metabolites was determined by LCMS. As shown in Fig. 9C, compound 21

reduced intracellular lactate levels at both 6 h and 24 h time points, demonstrating the functional effect of the LDHA inhibitor in cells. The changes in  $\alpha$ -ketoglutaric acid, citric acid, isocitric acid,

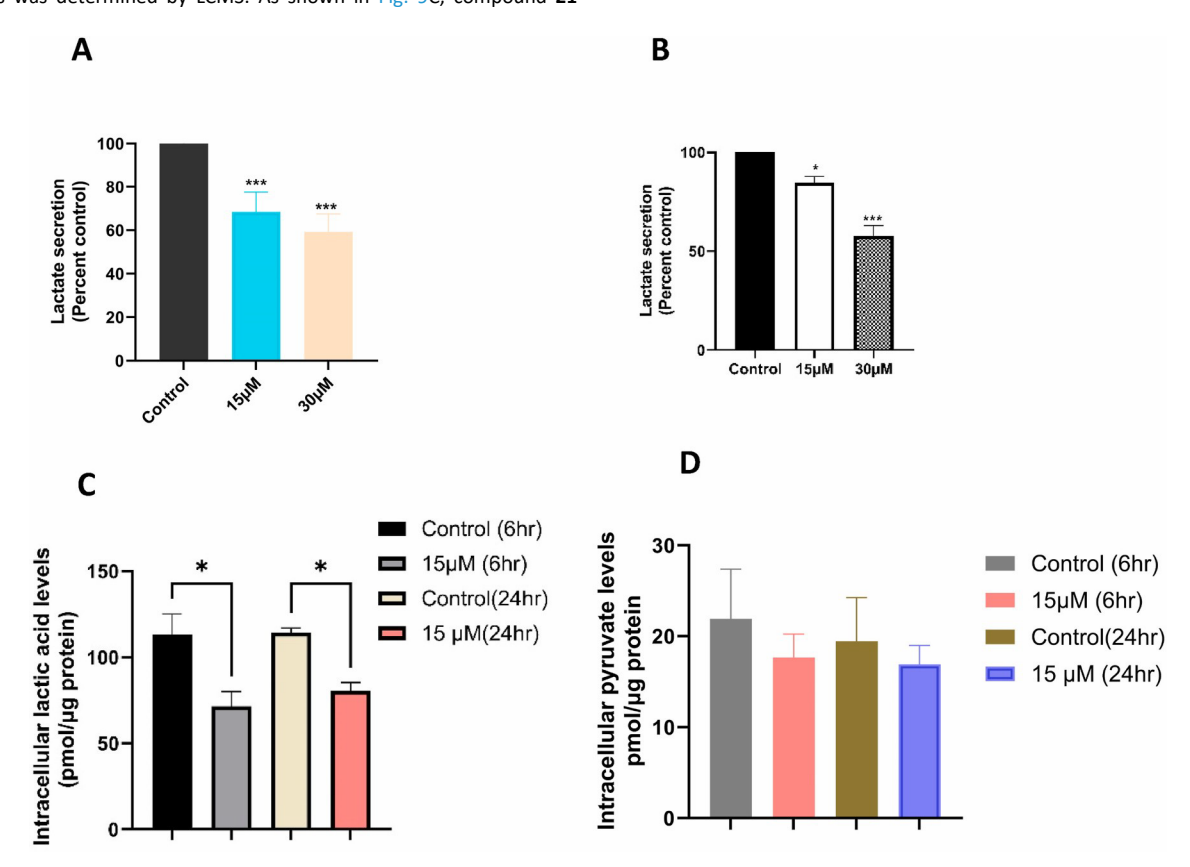


Fig. 9. (A) and (B) compound 21 reduced the extracellular lactate secreted in the culture media after 6 hpf treatment in MIA PaCa-2 cells compared to the untreated control. (A) cells were cultured in DMEM media comprising 25 mM glucose, 2 mM glutamine, and 1 mM pyruvate. (B) cells were cultured in DMEM media comprising 10 mM glucose, 2 mM glutamine without pyruvate. (C) compound 21 reduced intracellular lactate levels after 6 h and 24 h of treatment in MIA PaCa-2 cells as compared to the untreated control in the metabolomics assay. (D) Effect of compound 21 on the intracellular pyruvate levels in MIA PaCa-2 cells after 6 h and 24 h of treatment. Data is represented as mean ± SEM from n = 3 (\*p < 0.05, \*\*\*p < 0.001, one-way ANOVA).

succinate, malate, fumaric acid, and oxaloacetic acid are shown in the supplementary information, Fig. S6. For most metabolites there were no evident changes at either the 6 h or 24 h timepoint with respect to their untreated control, respectively. The LDHA inhibitor treatment reduced citric and isocitric acid levels in the 24-h timepoint samples compared to the control. However, the reduction of succinic acid levels in 21-treated cells was significant at the 6-h treatment time point. Overall, the results indicate that compound 21 does not substantially affect or upregulate the TCA cycle metabolites, but the effect on OXPHOS cannot be ruled out. The change in pyruvate levels is shown in Fig. 9D. The reduction in pyruvate levels is not statistically significant, but the decrease in pyruvate could be attributed to inhibition of glycolysis and glucose uptake upon inhibition of LDHA.

# 2.7. Compound 21 inhibits glycolysis and ATP production

We carried out a Seahorse glycolysis rate assay to assess the real-time changes in the glycolytic flux measured by the glyco-proton efflux rate (PER) upon LDHA inhibition [33]. The assay determines the net glycolysis-dependent proton production in the cells, which is a quantitative measure of the lactate produced solely by glycolysis. Inhibition of mitochondrial function by Rotenone and Antimycin A (Rot/AA) enables the calculation of mitochondrial-associated acidification. Subtraction of mitochondrial acidification to Total Proton Efflux

Rate results in Glycolytic Proton Efflux Rate. Consequently, a reduction of glycol-PER upon inhibitor treatment indicated inhibition of glycolysis and inhibition of LDHA. MIA PaCa-2 cells were treated with 10  $\mu$ M, 15  $\mu$ M, and 30  $\mu$ M concentrations of compound 21 for 6 h, and the changes in glyco-PER were monitored over 60 min (Fig. 10A). From glyco-PER, the effect of the compound in inhibiting basal and compensatory glycolysis was determined. Basal glycolysis is the initial PER measured after compound treatment but before adding drugs Rotenone + Antimycin A. Upon exposure to mitochondrial inhibitors and inhibition of OXPHOS, the rate of glycolysis increases to meet energy and biosynthetic demands. The assay records this increase in glycoPER as compensatory glycolysis. Compound 21 inhibited basal (Fig. 10B) and compensatory glycolysis (Fig. 10C) at 15  $\mu$ M, and 30  $\mu$ M concentrations, respectively. The reduction of glyco-PER by 21 correlates with LDHA inhibition, reduction of lactate secretion, and intracellular lactate levels.

The effect of 21 on the bioenergetics and rate of ATP production from glycolysis and mitochondrial OXPHOS (Fig. 11A) in MIA PaCa-2 cells was determined in the Seahorse ATP rate assay. Treatment of compound at 15  $\mu M$  and 30  $\mu M$  concentrations after 24 h reduced the total ATP production rate, including the glycolytic ATP production rate. Next, we determined the effect of compound 21 in inhibiting cell viability and ATP production in MIA PaCa-2 cells in the CellTiter-Glo assay.

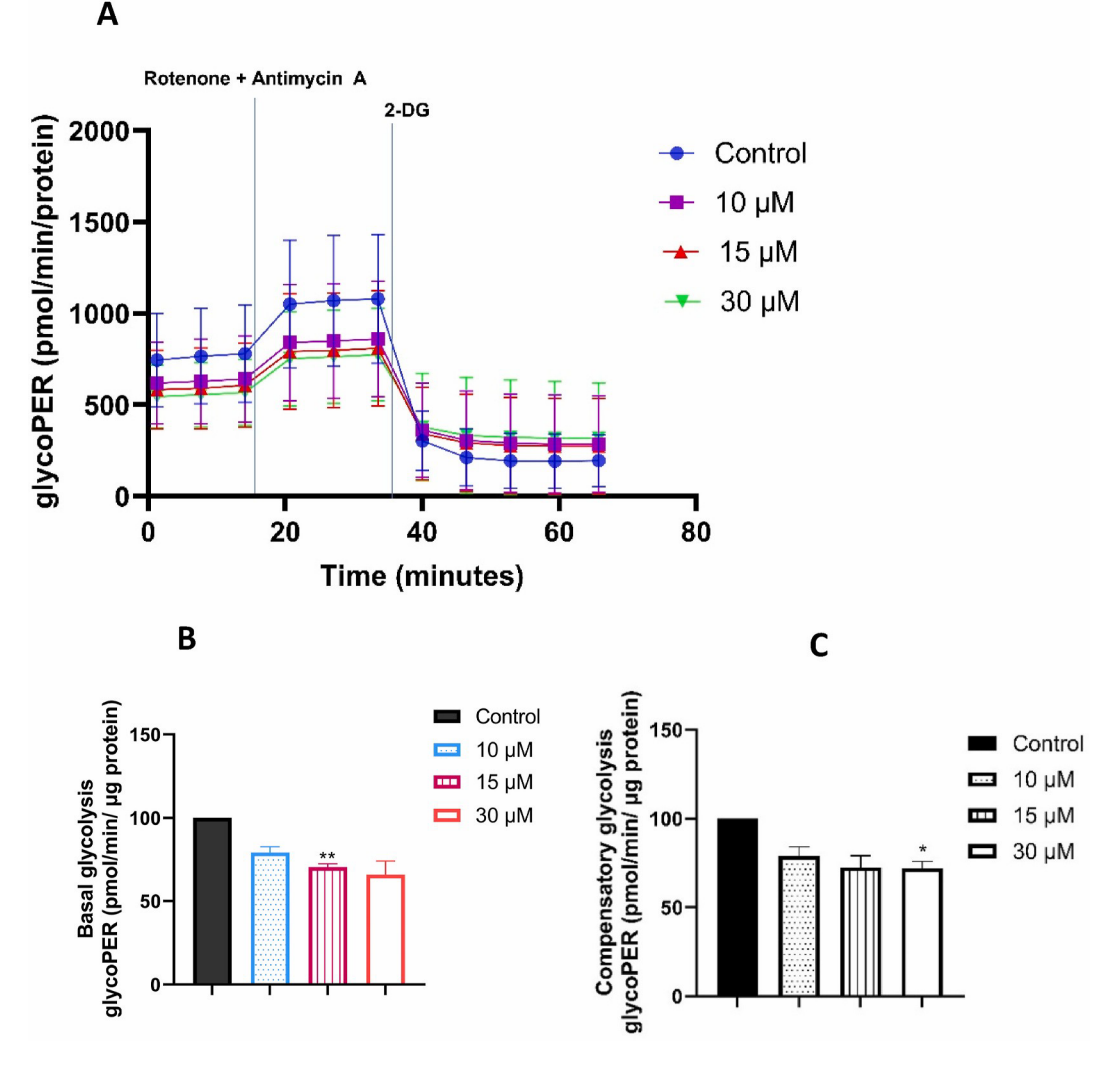
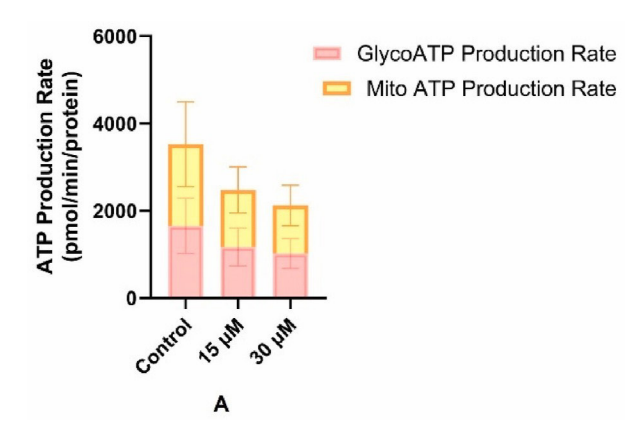


Fig. 10. Seahorse glycolytic rate assay. (A) MIA PaCa-2 cells were treated with 21 for 6 h, and the changes in the glyco PER were measured before and after the addition of drugs, Rotenone + Antimycin and 2-DG, until over 60 min. Compound 21 reduces (B) basal and (C) compensatory glycolysis compared to the untreated control. Data represent mean ± SEM (n = 3) (\*p < 0.05, \*\*p < 0.01, one-way ANOVA).



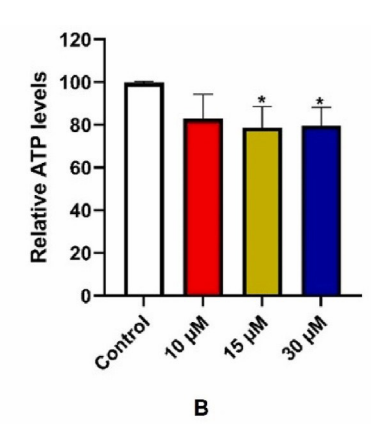


Fig. 11. Effect of compound 21 on ATP production. (A) In the Seahorse ATP rate assay, 21 reduced the total ATP production rate, including glycolysis ATP production rate, in MIA PaCa-2 cells after 24 h compared to the untreated control. (B) in the CellTiter-Glo assay, 21 reduced the intracellular ATP levels relative to untreated control after 48 h of treatment. Data represent mean ± SEM (n = 3) (\*p < 0.05, one-way ANOVA).

Treatment of 15  $\mu$ M and 30  $\mu$ M concentrations reduced ATP production after 48 h (Fig. 11B). However, the reduction at 10  $\mu$ M was not significant. It is to be noted that measuring cell viability using ATP assay for metabolic inhibitors could be context-dependent and may lead to underestimation of potency [34].

# 2.8. Antiproliferative and synergistic cell-kill in pancreatic cancer cell lines and patient-derived 3D organoids

Compounds **6** and **21** showed comparable antiproliferative effects against human pancreatic cancer cell lines PANC-1 and MIA PaCa-2. Compounds also inhibit the proliferation of mouse pancreatic cancer FC1199 cells, which were derived from tumors from KPC genetically engineered mice (Table 2) [35]. Cells were treated with compounds for 48 h, after which the live cells were counted using a fluorescence-based high-content confocal imaging system. Compound **21** showed an IC $_{50}$  value of 14  $\mu$ M against MIA PaCa-2 cells and did not display non-specific cytotoxicity against normal pancreatic cells, HPNE. We determined the expression of LDHA in all four cell lines by Western blotting (Fig. S7), which correlated with the cytotoxicity observed in the cell lines. Specifically, LDHA expression was highest in MIA PaCa-2 cells, followed closely by PANC-1, and the abundance was lowest in the normal HPNE cells. A plot of dose and % viable MIA PaCa-2 cell counts for **6** and **21** is shown in Fig. 12.

It is likely that inhibition of aerobic glycolysis may cause cancer cells to compensate and increase ATP via OXPHOS, the other source of energy production and cell survival [36]. Since a combination of LDHA-OXPHOS inhibitors could be more effective, we also tested whether the combination of 21 and phenformin, an OXHOS inhibitor, may show a synergistic effect. We evaluated the combination of 15  $\mu$ M and 20  $\mu$ M concentrations of 21 (IC $_{50}$  concentration) with 500  $\mu$ M-1000  $\mu$ M phenformin, the cytotoxic concentration range of phenformin reported in the literature. As shown in Fig. 13, compound 21 (20  $\mu$ M) demonstrated synergy of cell kill with phenformin (500  $\mu$ M), after 48 h of treatment in MIA PaCa-2 cells using a fluorescence-based high-content confocal imaging system. The effect of other combinations is

Table 2  $\mbox{Antiproliferative } \mbox{IC}_{50} \mbox{ values of compounds. } \mbox{Compound Cell}$ 

Proliferation IC <sub>50</sub> ± SD (μΜ) <sup>6</sup>									
	PANC-1	MIA PaCa-2	FC-1199	HPNE					
5	>50	24.213 ± 3.4	23.374 ± 3.5	26.458 ± 4.4					
6	23.944 ± 1.8	25.552 ± 2.7	12.121 ± 1.2	49.471 ± 7.3					
21	43.31 ± 3.98	14.12 ± 2.216	20.827 ± 2.97	>50					

 $<sup>^{\</sup>rm a}$  The IC  $_{\rm 50}$  values represent an average of three independent experiments, each conducted in, triplicate, and reported as  $\pm\,$  SD.

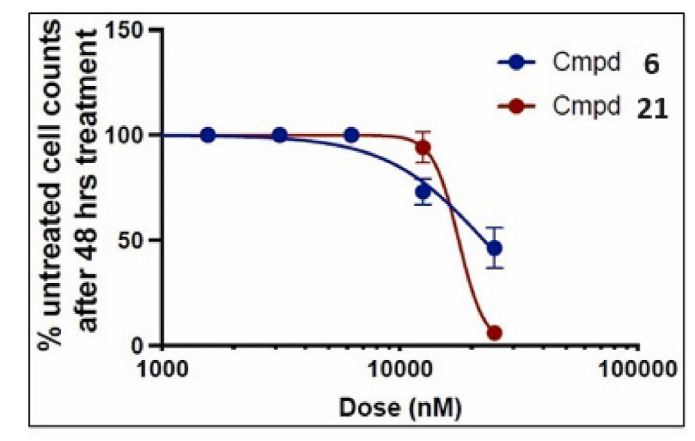


**Fig. 12.** Compounds **6** and **21** inhibit the proliferation of MIA PaCa-2 cells. Cells were treated with varying concentrations of compounds for 48 h and cell count were determined using Operetta image cytometer (n = 3).

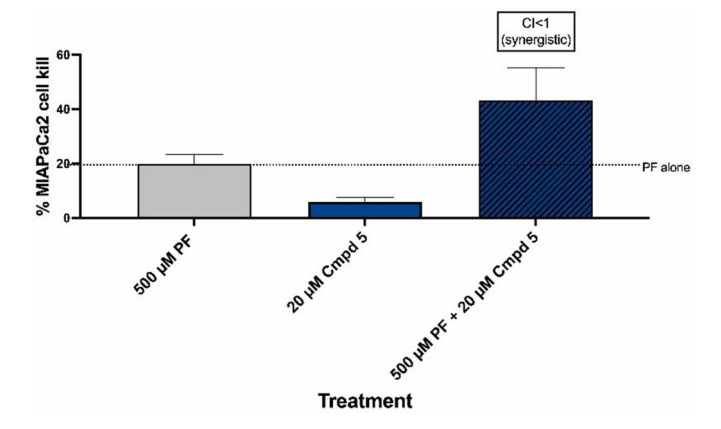


**Fig. 13.** Compound **21** (20  $\mu$ M) showed synergy with phenformin (PF) (500  $\mu$ M) in the proliferation assay in MIA PaCa-2 cells after 48 h. Synergy was determined using the Chou-Talalay method with a combination index (CI) < 1 (n = 3).

shown in the supplementary information, Fig. S8.

Next, we evaluated compounds **6** and **21** in *3D patient-derived* pancreatic cancer organoids, which better mimic the morphological, pathophysiological, and genomic features of the original patient tumor. Pancreatic cancer organoids (PANC137) were treated with indicated concentrations (5  $\mu$ M, 10  $\mu$ M, 25  $\mu$ M, 50  $\mu$ M, and 250  $\mu$ M) of compounds **6** and **21** along with vehicle control for 72 h. The survival of organoids was determined using the MTS CellTiter 96® AQueous One Solution cell proliferation assay. Compounds **6** and

**21** repressed the growth of pancreatic cancer organoids with equal potency (IC $_{50s}$  of 32.65  $\mu$ M and 32.34  $\mu$ M, respectively). The dose-response curve and representative bright-field image, showing the antiproliferative effect of compounds **6** and **21**, is shown in Fig. 14.

# 2.9. Microsomal stability, pharmacokinetic evaluation, and in vivo metabolic profiling

Since compound **6** is a methyl ester, it is expected to hydrolyze to the corresponding acid metabolite, compound **21**. Compounds **21** possess good aqueous solubility, good ligand efficiency, and ligand lipophilic efficiency (Table 3) and showed appreciable metabolic stability in both human and mouse liver microsomes (Table 4), with *in vitro* half-life of

>1 h and low intrinsic clearance of <0.0231 mL/min/mg protein in human and mouse plasma. The pharmacokinetics of compounds **6** and **21** were evaluated in male CD-1 mice following intravenous (IV) and peroral (PO) administration. Compounds **6** and **21** showed good oral bioavailability of 33% and 73%, respectively. Compound **21** also showed good systemic exposure (Table **5**) (36  $\mu$ M), low clearance (3.7 mL/min/Kg), achieving concentration in the range of cellular IC<sub>50</sub> after PO dosing at 5 mg/kg dose. Further, compound **21** showed a moderate  $t_{V_2}$  of 2.4 h. In the PK analysis of **6**, we also quantified the formation of compound **21** in vivo (Table 6). Administration of **6** will likely result in a cumulative effect from the parent ester compound and its active acid-metabolite, compound **21**, resulting in a cumulative  $t_{1/2}$  of 4.5 h. We also quantified potential metabolites of **21** (Fig. 15) by LC-MS/MS in the blood plasma samples over time after a single dose. However, either a very weak signal or no signal was detected, or the signal registered does not confirm the presence of a metabolite, suggesting metabolically

Table 3

Physicochemical properties of compound 21.

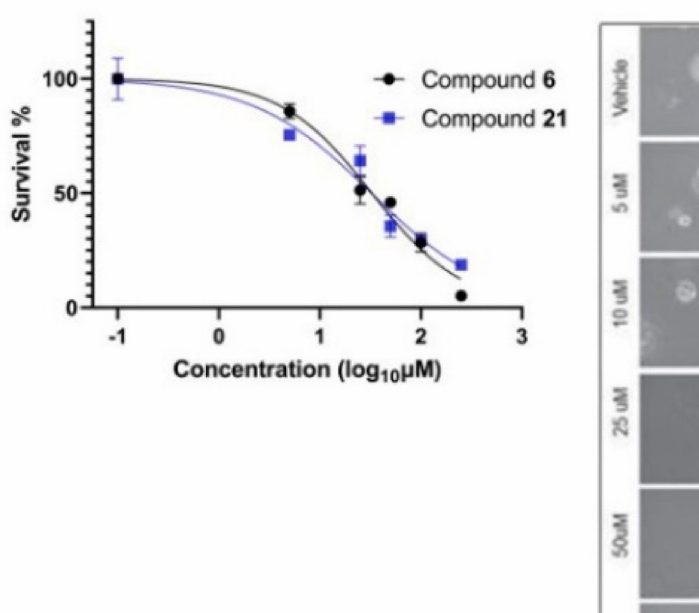
Compound	Mol wt.	logP	Ligand efficiency <sup>a</sup>	Ligand lipophilic efficiency <sup>b</sup>	Thermodynamic solubility, (µg/mL), (pH 7.4, PB)
21	445.4	2.47	0.305	4.67	7685

- Caclulated from LDHA pIC<sub>50</sub>.
- b Calulated from logP value from Chemaxon. stability of

compound 21.

### 3. Conclusions

In this study, we synthesized succinic acid monoamide derivatives and explored the SAR, identifying related compounds **6** and **21** as potent LDHA inhibitors. The methyl ester (**6**) and the acid derivative (**21**) showed similar effects and exhibited potent inhibition of LDHA. We confirmed LDHA binding affinity by SPR and solved two crystal structures of our inhibitor with LDHA. Compounds inhibit lactate production, ATP, and glycolysis, cause suppression of the growth of pancreatic cancer cell lines and patient-derived 3D organoids, and exhibit synergy with OXPHOS inhibitor phenformin. Additionally, **6** and **21** showed excellent metabolic stability and PK properties with good oral bioavailability. Since the administration of **6** would form **21** *in vivo*, compound **6** resulted in a cumulative half-life of over 4.5 h following administration in mice. The succinic acid monoamide class of inhibitors could be further developed as a drug-like lead to explore the translational benefit of simultaneously inhibiting lactate production and OXHPOS in PDAC.



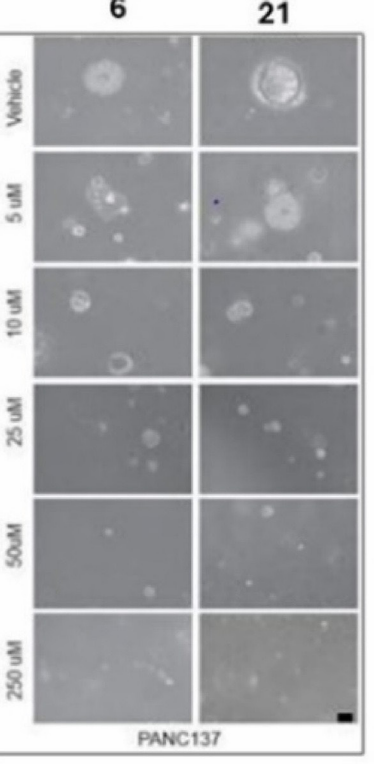


Fig. 14. Effect of compounds 6 and 21 on pancreatic cancer organoids (PANC137). (A) Dose-response curve for 6 and 21 showing the antiproliferative effect and inhibition of the growth of pancreatic cancer organoids; (B) Suppression of growth of pancreatic cancer organoids (PANC137B) shown by bright-field image at 200x magnification after treatment of compounds 6 and 21 at indicated concentrations for 48 h.

Table 4
In vitro microsomal stability of compound 21.

Compound	Microsomal stability	Percentage remaining of initial					t <sub>1/2</sub> (min)	Cl <sub>int</sub> (mL/min/mg protein)
		0	0 10 20 30 60			60		
21	Human	100	95.5	94.8	90.5	75.6	>60	<0.0231

73 %

1	Mouse	100	98.6	96.0	98.0	88.4	>60	< 0.0231

36.44

Table 5

Oral

Pharmacokinetics of compound <b>21</b> in male CD-1 nice.								
Compound 21	Dose (mg/kg)	T <sub>max</sub> (min)	$C_{max}(\mu M)$	$AUC_0 \mathop{\rightarrow}_{\!$	t1/2 (h)	CL (mL min <sup>-1</sup> Kg <sup>-1</sup> )	V <sub>d</sub> (L/Kg)	F (bioavailability
IV	1	-	21.17	10.01	2.9	3.7	0.9	

2.4

Table 6

Pharmacokinetic evaluation of compound 6 and its metabolite (compound 21) formed in v. vo.

10.44

30

That made and the compound of and its metabolite (compo				==,					
	Route	Dose (mg/kg)	T <sub>max</sub> (min)	$C_{\text{max}}(\mu M)$	$AUC_0 \!\to\!$	t <sub>1/2</sub> (h)	CL (mL min <sup>-1</sup> Kg <sup>-1</sup> )	V <sub>d</sub> (L/Kg)	F
Compound 6	IV	1	-	1.02	0.328	1.19	110	10	
metabolite (21)			30	1.01	4.04	2.18			
Compound 6 metabolite (21)	Oral	5	15 30	0.48 9.76	0.551 25.96	1.63 2.92	-	-	33 %

# Amide hydrolysis, N-glucuronide Reduction, glucuronride, sulfate comjugation hydroxylation HN N-dealkylation

Fig. 15. Metabolic profiling of compound 21 investigated in mice.

# 4. Experimental

# 4.1. Chemistry

All reagents and solvents were purchased from commercial sources and used without further purification. The progress of all reactions was monitored by analytical thin-layer chromatography, which was performed on aluminumbacked silica-gel 60 F254 plates. Compounds were purified by flash purification using a Biotage Isolera system by gradient elution of hexanes and ethyl acetate (EtOAc) or dichloromethane (DCM) and methanol mixture. <sup>1</sup>H and <sup>13</sup>C NMR spectra were recorded on a Bruker AVANCE II 300 spectrometer at 300 MHz and 75 MHz, respectively. Proton chemical shifts are reported in parts per million ( $\delta$ ) relative to TMS or the known chemical shift of the solvent as the spectral reference. The electrospray ionization mass spectroscopy was performed using a Shimadzu LCMS-2020 single quadrupole LC-MS spectrometer. All final compounds screened in biological assays showed a purity >95% by HPLC analysis, except compound 19 (91.7%). The purity of all compounds tested in biological assays was determined by high- performance liquid chromatography (HPLC) using (a) Agilent 1100 system with Hamilton PRC C-18, 5  $\mu$ m, 4.6 mm  $\times$  150 mm reverse-phase analytical column. Solvent A (0.1% TFA in  $H_2O$ ) and solvent B (0.1% TFA in  $CH_3CN$ ) as eluents was used in an isocratic elution of 30:70 water/CH<sub>3</sub>CN with an injection volume of 2 μL at a flow rate of 1.5 mL/ min for 10 min; or (b) Shimadzu/Agilent HPLC system using Sinochrom ODS-BP (4.6 mm  $\times$  250 mm, 5  $\mu$ m) column with column temperature set at 30 °C. The mobile phase, which consisted of 0.1% TFA in water (A) and 0.1% TFA in CH<sub>3</sub>CN (B), was applied with the following gradient: 0.01–20 min, 30%–100% B; 20–25.00 min, 100% B. The flow rate was set at 1.0  $\,$ mL/min for 25 min, and the injection volume was 10 μL. UV-vis detection at 254/330 nm (method a) or at 220 nm (method b) was recorded. Method b was used for purity analysis for the final compounds 19, 23, 24, 29, 33, 34, 35, and **36**, while all remaining test compounds were analyzed using HPLC method a. High-resolution mass spectra were acquired using the Agilent 6546 QTOF at the

OU Mass Spectrometry, Proteomics & Metabolomics Core facility. Melting points (Mp) of final test compounds were determined using a DigiMelt melting point apparatus.

# 4.1.1. General procedure for the preparation of intermediate II (2a-2f)

Example para-trifluoro methyl phenyl (R1 substituent) acetic acid was converted to the corresponding methyl ester intermediate II, compound 2b. To a stirred solution of 2-(4-(trifluoromethyl)phenyl)acetic acid (2.0 g, 9.79 mmol, 1 equiv) in methanol (20 mL), was added H2SO4 (0.2 mL). The reaction mixture was stirred at room temperature (rt) for 2 h. After the reaction, the reaction mixture was concentrated and quenched with saturated NaHCO3. The organic layer was washed with brine and extracted with DCM. The organic layer was then dried over Na2SO4 and evaporated in vacuo. The crude product was purified by flash chromatography using hexanes/EtOAc (5–20% EtOAc) as the eluent.

# 4.1.2. General procedure for the preparation of intermediate III (3a-3f)

Intermediates II, example compound **2b** with *para*-trifluoro methyl phenyl (R<sub>1</sub> substituent), was converted to the corresponding *tert*-butyl ester, intermediate III, compound **3b**. Methyl 2-(4-(trifluoromethyl) phenyl)acetate (6.0 g, 27.5 mmol, 1 equiv) was slowly added to a stirred solution of lithium diisopropylamide generated *in situ* from *n*-BuLi (1.6 M) (18.68 mL, 1.02 equiv) and diisopropyl amine (4.3 mL, 1.05 equiv) in 80 mL of dried THF. The solution was stirred for 45 min at – 78 °C, and *tert*-butyl bromoacetate (13.08 mL, 3 equiv) was added dropwise. The resulting solution was stirred for 20 min at – 78 °C and then allowed to come to rt and stirred for 4 h. The reaction was quenched with saturated NH<sub>4</sub>Cl, concentrated to a small volume, washed with brine, and extracted with EtOAc. The organic layer was dried over Na<sub>2</sub>SO<sub>4</sub> and evaporated to dryness. The crude product was purified by flash chromatography using hexanes/EtOAc (10–50% EtOAc) as the eluent.

# 4.1.3. General procedure for the preparation of intermediate IV (4a-4f)

The *tert*-butyl ester intermediate III, for example, compound **3b** with *para*-trifluoro methyl phenyl (R<sub>1</sub> substituent), was converted to the corresponding acid, intermediate IV, compound **4b**. To a stirred solution of 4-(*tert*-butyl) 1-methyl 2-(4-(trifluoromethyl)phenyl) succinate (R<sub>1</sub> = para-CF<sub>3</sub>) (4.5 g, 13.54 mmol) in DCM (15 mL) was added TFA (15 mL). The reaction mixture was stirred at room temperature for 3 h. The reaction was concentrated and the TFA was removed with the addition of toluene to obtain a solid crude. The crude product was purified by flash chromatography using hexanes/EtOAc (30–70% EtOAc) as the eluent.

# 4.1.4. General procedure for the preparation of **V** (compounds $\mathbf{5}$ – $\mathbf{19}$ ) (method $\mathbf{A}$ )

Acid intermediate IV, example 4a, (0.2 g, 0.824 mmol) was dissolved in anhydrous DCM (2 mL) and a few drops of DMF. The reaction mixture was cooled on an ice bath and oxalyl chloride (0.1 mL, 1.5 equiv) was added dropwise. The mixture was stirred in ice for 15 min and allowed to come to rt for over 2 h. The reaction mixture was concentrated and dried in vacuo. The resulting acid chloride was added to a solution of (4- aminophenyl)(1-methyl-1H-imidazole-2-yl)methanone (0.138 g, mmol, 0.689 mmol, 0.9 equiv) and triethyl amine (0.14 mL, 1.3 equiv) in DCM (3 mL) and a few drops of DMF. The reaction was stirred at rt for 24 h. After completion of the reaction, the reaction mixture was quenched with 0.1 N HCl, and the aqueous layer was extracted with DCM. The organic layer was washed with brine, dried over Na<sub>2</sub>SO<sub>4</sub>, and concentrated in vacuo. The crude product was purified by flash chromatography using hexanes/EtOAc (40–80% EtOAc) as the eluent.

**Method B**. Intermediate **IV**, example **4b**, (2.0 g, 7.24 mmol, 1 equiv), HATU (Hexafluorophosphate Azabenzotriazole Tetramethyl Uronium) (2.75 g, 7.24 mmol, 1 equiv), and (4-aminophenyl)(1-methyl- 1H-imidazol-2-yl)methanone (1.46 g, 7.24 mmol, 1 equiv) was added to DCM (10 mL). Triethylamine (3.03 mL, 3 equiv) was added to the reaction mixture, which was stirred at rt for 48 h. After the reaction, the reaction mixture was extracted with DCM. The organic layer was washed with brine, dried over  $Na_2SO_4$ , and concentrated under reduced pressure. The crude product was purified by flash chromatography using hexanes/EtOAc (40–80% EtOAc) as the eluent.

# 4.1.5. General procedure for the preparation of $\emph{VI}$

Methyl esters in V were hydrolyzed to give the corresponding acid-containing compounds **20–28.** For example, compound **6** (0.4 g, 0.87 mmol, 1 equiv) was treated with lithium hydroxide (0.11 g, 2.61 mmol, 3 equiv) in THF-water (4 mL:1 mL) and the reaction mixture was stirred at room temperature for 2 h. After the reaction, HCl was added to adjust the pH to 4. The reaction mixture was concentrated and extracted with DCM. The organic layer was dried over  $Na_2SO_4$  and evaporated to dryness. The crude product was purified by preparative TLC or flash chromatography using MeOH/DCM (1–5% MeOH) as the eluent.

**methyl 2-(4-chlorophenyl)acetate (2a)**. Compound **2a** was prepared according to the general procedure for the preparation of **II**. 2.0 g (11.72 mmol) of 2-(4-chlorophenyl)acetic acid afforded 1.91 g (88.4%) of **2a** as colorless liquid. ESI-MS m/z [M + H]<sup>+</sup> = 185.  $^{1}$ H NMR (300 MHz, CDCl<sub>3</sub>)  $\delta$  7.29 (d, J = 9.0 Hz, 2H), 7.21 (d, J = 9.0 Hz, 2H), 3.69 (s, 3H), 3.6 (s, 2H).

methyl 2-(4-(trifluoromethyl)phenyl)acetate (2b). Compound 2b was prepared according to the general procedure for the preparation of II. 2-(4-(trifluoromethyl)phenyl)acetic acid (2.0 g, 9.79 mmol) afforded 1.92 g (90.1%) of 2b as colorless liquid. ESI-MS m/z [M - H] $^+$  = 217.  $^1$ H NMR (300 MHz,

of **2b** as colorless liquid. ESI-MS m/z [M - H]<sup>+</sup> = 217. <sup>1</sup>H NMR (300 MHz, Methanol- $d_4$ )  $\delta$  7.41 (d, J = 9.0 Hz, 2H), 7.48 (d, J = 6.0 Hz, 2H), 3.77 (s, 2H), 3.7 (s, 3H). methyl **2-(4-methoxyphenyl)acetate** (**2c**). Compound **2c** was prepared

according to the general procedure for the preparation of II. 2.0 g (12.03 mmol) of 2-(4-methoxyphenyl)acetic acid afforded 1.85 g (85.5%) of **2c** as colorless liquid. ESI-MS m/z [M + H]<sup>+</sup> = 181.<sup>1</sup>H NMR (300 MHz, CDCl<sub>3</sub>)  $\delta$  7.19 (d, J = 9.0 Hz, 2H), 6.86 (d, J = 9.0 Hz, 2H), 3.79 (s, 3H), 3.68 (s, 3H), 3.57 (s, 2H).

methyl 2-(2-phenylthiazol-4-yl)acetate (2d). Compound 2d was prepared according to the general procedure for the preparation of II. 2.0 g (9.12 mmol) of 2-(2-phenylthiazol-4-yl)acetic acid afforded 1.85 g

(87.3%) of **2e** as colorless liquid. ESI-MS m/z [M + H]<sup>+</sup> = 234.  $^{1}$ H NMR (300 MHz, Methanol- $d_4$ )  $\delta$  7.90–7.03 (m, 2H), 7.43–7.46 (m, 3H), 7.38 (s, 1H), 3.90 (s, 2H), 3.74 (s, 3H).

**methyl 2-phenylacetate** (**2e**). Compound **2e** was prepared according to the general procedure for the preparation of **II**. 2.0 g (14.68 mmol) of 2-phenylacetic acid afforded 1.87 g (84.2%) of **2e** as colorless liquid. [M – H] $^+$  = 149.  $^1$ H NMR (300 MHz, CDCl $_3$ )  $\delta$  7.26–7.32 (m, J = 5H), 3.68 (s, 3H), 3.62 (s, 2H).

methyl 2-(4-fluorophenyl)acetate (2f). Compound 2f was prepared according to the general procedure for the preparation of II. 6.0 g (38.95 mmol) acid afforded 5.64 g (86.3%) of 2f as colorless liquid. ESI-

MS m/z [M + H]<sup>+</sup> = 181.<sup>1</sup>H NMR (300 MHz, CDCl<sub>3</sub>)  $\delta$  7.19 (d, J = 9.0 Hz, 2H), 6.86 (d, J = 9.0 Hz, 2H), 3.79 (s, 3H), 3.68 (s, 3H), 3.57 (s, 2H).

**4-(tert-butyl) 1-methyl 2-(4-chlorophenyl)succinate** (**3a**). Compound **3a** was prepared according to the general procedure for the preparation of intermediate **III.** 0.676 g (3.66 mmol) of *methyl 2-(4- chlorophenyl)acetate* afforded 0.55 g (50.9% yield) of **3a** as white solid. ESI-MS m/z [M + 23] = 321.  $^1$ H NMR (300 MHz, CDCl<sub>3</sub>)  $\delta$  7.29 (d, J =

6.0 Hz, 2H), 7.23–7.20 (d, J = 9.0 Hz, 2H), 4.0 (dd, J = 9.0, 6.0 Hz, 1H), 3.67 (s, 3H), 3.07 (dd, J = 18.0, 9.0 Hz, 1 H), 2.58 (dd, J = 15.0, 6.0 Hz, 1H), 1.40 (s, 9H).

**4-(tert-butyl) 1-methyl 2-(4-(trifluoromethyl) phenyl)succinate** (**3b**). Compound **3b** was prepared according to the general procedure for the preparation of intermediate **III.** (0.925 g, 4.23 mmol) of *methyl* 2-(4-(trifluoromethyl)phenyl)acetate afforded 1.0 g (71.0%) of **3b** as white solid. ESI-

MS m/z [M - H]<sup>+</sup> = 331. <sup>1</sup>H NMR (300 MHz, CDCl<sub>3</sub>)  $\delta$  7.55–7.62 (m, 2H), 7.37–7.45 (m, 2H), 4.05–4.12 (m, 1H), 3.68 (s, 3H), 3.03–3.16 (m, 1 H), 2.52–2.66 (m, 1H), 1.40 (s, 9H).

**4-(***tert***-butyl) 1-methyl 2-(4-methoxyphenyl) succinate** (**3c**). Compound **3c** was prepared according to the general procedure for the preparation of intermediate **III**. 6.0 g (33.3 mmol) of methyl 2-(4- methoxyphenyl)acetate, afforded 4.5 g (45.9%) of **3c** as white solid. ESI- MS m/z [M + 23] = 317.  $^1$ H NMR (300 MHz, CDCl<sub>3</sub>)  $\delta$  7.20 (d, J = 6.0 Hz, 2H), 6.84 (d, J = 9.0 Hz, 2H), 3.97 (dd, J = 10.5, 4.5 Hz, 1H), 3.78 (s, 3H), 3.66 (s, 3H), 3.07 (dd, J = 16.5, 10.5 Hz, 1H), 2.57 (dd, J = 18.0, 6.0 Hz, 1H), 1.40 (s, 9H).

**4-(tert-butyl) 1-methyl 2-(2-phenylthiazol-4-yl) succinate** (**3d**). Compound **3d** was prepared according to the general procedure for the preparation of intermediate **III**. 1.8 g (7.71 mmol) of *methyl* **2-(2-phenylthiazol-4-yl)acetate** afforded 2.4 g (89.5%) of **3d** as yellow solid. ESI- MS m/z [M + 23] = 370.  $^1$ H NMR (300 MHz, CDCl<sub>3</sub>)  $\delta$  7.90–7.94 (m, 2H), 7.40–7.43 (m, 3H), 7.11 (s, 1H), 4.36 (dd, J = 9.0, 6.0 Hz, 1H), 3.73

(s, 3H), 3.16 (dd, J = 16.5, 10.5 Hz, 1H), 2.89 (dd, J = 18.0, 6.0 Hz, 1H), 1.43 (s, 9H).

**4-(tert-butyl) 1-methyl 2-phenylsuccinate** (**3e**). Compound **3e** was prepared according to the general procedure for the preparation of intermediate **III**. 1.0 g of methyl 2-phenylacetate (6.65 mmol) afforded 1.3 g (73.8%) of **3e** as a light-yellow solid.  $^1$ H NMR (300 MHz, CDCl<sub>3</sub>)  $\delta$  7.25–7.35 (m, 5H), 4.0–4.04 (m, 1H), 3.67 (s, 3H), 3.07–3.17 (m, 1H), 2.57–2.63 (m, 1H), 1.40 (s, 9H).

**4-(tert-butyl) 1-methyl 2-(4-fluorophenyl) succinate** (**3f**). Compound **3f** was prepared according to the general procedure for the preparation of intermediate **III.** 5.6 g (33.3 mmol) of methyl 2-(4-fluorophenyl)acetate afforded 4.32 g (45.9%) of **3f** as yellow solid. ESI-MS m/z [M - H] = 281.  $^{1}$ H NMR (300 MHz, CDCl<sub>3</sub>)  $\delta$  7.25–7.30 (m, 2H), 7.0–7.05 (m, 2H), 4.04 (dd, J = 10.5, 4.5 Hz, 1H), 3.7 (s, 3H), 3.11 (dd, J = 16.5, 10.5 Hz, 1H), 2.63 (dd, J = 18.0, 6.0 Hz, 1H), 1.42 (s, 9H).

**3-(4-chlorophenyl)-4-methoxy-4-oxobutanoic acid (4a)**. Compound **4a** was prepared according to the general procedure for the preparation of **IV.** 1.67 g (5.59 mol) of 4-(*tert*-butyl) 1-methyl 2-(4-chlorophenyl)succinate afforded 1.28

g (94.4%) of **4a** as off-white solid. ESI-MS m/z [M – H]<sup>+</sup> = 241. <sup>1</sup>H NMR (300 MHz, CDCl<sub>3</sub>)  $\delta$  7.30 (d, J = 9 Hz, 2H), 7.25 (d, J = 9 Hz, 2H), 4.03 (dd, J = 10.5, 4.5 Hz, 1H), 3.68 (s, 3H), 3.22 (dd, J = 16.5, 10.5 Hz, 1H), 2.5 (dd, J = 18.0, 6.0 Hz, 1H).

**4-methoxy-4-oxo-3-(4-(trifluoromethyl)** phenyl)butanoic acid (**4b**). Compound **4b** was prepared according to the general procedure for the preparation of **IV.** 4.5 g (13.54 mmol) of 4-(*tert*-butyl) 1-methyl 2-(4-(trifluoromethyl) phenyl)succinate afforded 2.99 g (79.9%) of **4b** as white solid.

ESI-MS m/z [M - H]<sup>+</sup> = 275. <sup>1</sup>H NMR (300 MHz, CDCl<sub>3</sub>)  $\delta$  7.53 (d, J = 9 Hz, 2H), 7.33 (d, J = 9 Hz, 2H), 4.06 (dd, J = 9.0, 6.0 Hz, 1H), 3.62 (s, 3H), 3.20 (dd, J = 18.0, 9.0 Hz, 1H), 2.67 (dd, J = 18.0, 6.0 Hz, 1H).

**4-methoxy-3-(4-methoxyphenyl)-4-oxobutanoic acid** (**4c**). Compound **4c** was prepared according to the general procedure for the preparation of **IV.** 1.2 g (4.07 mmol) of 4-(tert-butyl) 1-methyl 2-(4- methoxyphenyl) succinate afforded **4c** in quantitative yield as white solid. ESI-MS m/z [M + 23] = 261.  $^1$ H NMR (300 MHz, CDCl<sub>3</sub>)  $\delta$  7.19 (d, J = 9 Hz, 2H), 6.85 (d, J = 9 Hz, 2H), 4.0 (dd, J = 10.5, 4.5 Hz, 1H), 3.79 (s, 3H), 3.67 (s, 3H), 3.22 (dd, J = 18.0, 9.0 Hz, 1H), 2.68 (dd, J = 16.5, 4.5 Hz, 1H).

4-methoxy-4-oxo-3-(2-phenylthiazol-4-yl) butanoic acid (4d). Compound 4d was prepared according to the general procedure for the preparation of IV. 2.28 g (6.56 mmol) of 4-(tert-butyl) 1-methyl 2-(2- phenylthiazol-4-yl) succinate afforded 1.2 g (62.8%) of 4d as white solid. ESI-MS m/z [M – H] $^+$  = 290.  $^1$ H NMR (300 MHz, CDCl $_3$ )  $\delta$ 

7.80-7.84 (m, 2H), 7.35-3.37 (m, 3H), 7.20 (s, 1H), 4.34 (dd, J=9.0, 6.0 Hz, 1H), 3.68 (s, 3H), 3.26 (dd, J=16.5, 7.5 Hz, 1H), 2.98 (dd, J=18.0, 6.0 Hz, 1H).

**4-methoxy-4-oxo-3-phenylbutanoic acid (4e)**. Compound **4e** was prepared according to the general procedure for the preparation of **IV**. 1.01 g (3.82 mmol) of 4-(*tert*-butyl) 1-methyl 2-phenylsuccinate afforded 0.5 g (62.8%) of

**4e** as white solid. ESI-MS m/z [M - H] $^+$  = 207.  $^1$ H NMR (300 MHz, Methanol- $d_4$ )  $\delta$  7.28-7.37 (m, 5H), 4.07 (dd, J = 10.5, 4.5 Hz, 1H), 3.66 (s, 3H), 3.15 (dd, J = 18.0, 12.0 Hz, 1H), 2.69 (dd, J = 16.5, 4.5 Hz, 1H).

4-(tert-butyl) 1-methyl 2-(4-fluorophenyl) succinate (4f). Compound 4f was prepared according to the general procedure for the preparation of IV. 4.32 g (15.31 mmol) of 4-(tert-butyl) 1-methyl 2-(4- methoxyphenyl) succinate afforded 2.73 g (78.9%) of 4f as white solid. ESI-MS m/z [M- H] = 225.  $^1$ HNMR (300 MHz, DMSO- $d_6$ )  $\delta$  ppm 12.39

(bs, 1H), 7.34 (t, J = 7.5 Hz, 2H), 7.16 (d, J = 7.5 Hz, 2H), 4.03 (dd, J = 9.0, 6.0 Hz, 1H), 3.58 (s, 3H), 3.0 (dd, J = 16.5, 10.5 Hz, 1H), 2.63 (dd, J = 18.0, 6.0 Hz, 1H).

methyl 2-(4-chlorophenyl)-4-((4-(1-methyl-1H-imidazole-2-car bonyl)phenyl)amino)-4-oxobutanoate (5). Compound 5 was prepared according to the general procedure for the preparation of V using method A. 0.2 g (0.824 mmol) of 3-(4-chlorophenyl)-4-methoxy-4- oxobutanoic acid afforded 0.146 g (41.6%) of compound 5 as light yellow solid. Mp 161–164 °C.

ESI-MS m/z [M - H]\*  $_{\pm}$  424.  $^{1}$ H NMR (300 MHz, Methanol- $d_{4}$ )  $\delta$  8.02 (d, J = 9.0, 2H), 7.57 (d, J = 9.0, 2H), 7.16–7.28 (m, 5H), 7.05 (bs, 1H), 4.1 (dd, J = 9.0, 6.0 Hz, 1H), 3.92 (s, 3H), 3.58 (s, 3H), 3.0 (dd, J = 18.0, 9.0 Hz, 1H), 2.88 (dd, J = 15.0, 6.0 Hz, 1H). HRMS (ESI) m/z calculated for  $C_{22}H_{20}CIN_{3}O_{4}$ : 425.1142, found [M + H]\* 426.1220. **methyl** 4-((4-(1-methyl-1H-imidazole-2-carbonyl)phenyl)amin o)-4-oxo-2-(4-(trifluoromethyl)phenyl)butanoate (6). Compound 6 was prepared according to the general procedure for the preparation of **V** using procedure B. A reaction of 2.0 g (7.24 mmol) of 4-methoxy-4- oxo-3-(4-(trifluoromethyl) phenyl)butanoic acid afforded 2.2 g (66.1%) of compound **6** as light yellow solid. Mp 170–172 °C. ESI-MS m/z [M +

H]<sup>+</sup> = 460. <sup>1</sup>H NMR (300 MHz, DMSO- $d_6$ )  $\delta$  10.43 (s, 1H), 8.26 (d, J = 9.0 Hz, 2H), 7.73 (d, J = 9.0 Hz, 2H), 7.68 (d, J = 9.0 Hz, 2H), 7.55–7.58 (m, 3H), 7.18 (s, 1H), 4.29 (dd, J = 9.0, 6.0 Hz, 1H), 3.97 (s, 3H), 3.61 (s, 3H), 3.22 (dd, J = 18.0, 9.0 Hz, 1H), 2.55 (dd, J = 16.5, 4.5 Hz, 1H). <sup>13</sup>C NMR (75 MHz, Methanol-d4)  $\delta$  183.0, 173.17, 170.03, 143.09, 142.99, 142.59, 136.91, 132.19, 131.69, 128.56, 128.38, 128.0, 127.0, 126.18, 125.39, 118.19, 51.54, 37.49, 34.95. HRMS (ESI) m/z calculated for C<sub>23</sub>H<sub>20</sub>F<sub>3</sub>N<sub>3</sub>O<sub>4</sub>: 459.1406, found [M + H]<sup>+</sup> 460.1493.

methyl 4-((3-fluoro-4-morpholinophenyl)amino)-4-oxo-2-(4-(tr

**ifluoromethyl)phenyl)butanoate** (**7**). Compound **7** was prepared according to the general procedure for the preparation of **V** using method A. 0.1 g (0.362 mmol) of 4-methoxy-4-oxo-3-(4-(trifluoromethyl) phenyl)butanoic acid afforded 90 mg (54.8%) of compound **7** as white solid. Mp 156–159 °C. ESI-MS m/z [M - H] $^+$  = 453.  $^1$ H NMR (300 MHz, CDCl $_3$ )  $\delta$  7.60 (d, J = 6.0 Hz, 2H), 7.42 (d, J = 6.0 Hz, 2H), 7.37 (bs, 1H), 7.02 (d, J = 9.0 Hz, 1H), 6.85 (t, J = 9.0 Hz, 1H), 4.32 (dd, J = 9.0, 3.0 Hz, 1H), 3.85–3.88 (m, 4H), 3.69 (s, 3H), 3.21 (dd, J = 15.0, 9.0 Hz, 1H), 3.02–3.05 (m, 4H), 2.67 (dd, J = 16.5, 4.5 Hz, 1H). HRMS (ESI) m/z

methyl 4-((6-chloropyridazin-3-yl)amino)-4-oxo-2-(4-(trifluoro methyl)phenyl)butanoate (8). Compound 8 was prepared according to the general procedure for the preparation of V using method A. 0.25 g (0.90 mmol) of 4-methoxy-4-oxo-3-(4-(trifluoromethyl) phenyl)butanoic acid afforded 85 mg (24.2%) of compound 8 as orange solid. Mp 180–184 °C. ESI-MS m/z [M + 23] = 410. ¹H NMR (300 MHz, Methanol-  $d_4$ ) δ 8.46 (d, J = 9.0 Hz, 1H), 7.73 (d, J = 9.0 Hz, 1H), 7.67 (d, J = 9.0 Hz, 2H), 7.56 (d, J = 6.0 Hz, 2H), 4.34 (dd, J = 9.0, 6.0 Hz, 1H), 3.70 (s, 3H), 3.41 (dd, J = 15.0, 9.0 Hz, 1H), 2.92–3.0 (m, 1H). HRMS (ESI) m/z calculated for C<sub>16</sub>H<sub>13</sub>CIF<sub>3</sub>N<sub>3</sub>O<sub>3</sub>: 387.0598, found [M + H]\*388.0678.

calculated for  $C_{22}H_{22}F_4N_2O_4$ : 454.1516, found [M + H]+455.1595.

methyl 4-((4-benzoylphenyl)amino)-4-oxo-2-(4-(trifluorometh yl)phenyl)butanoate (9). Compound 9 was prepared according to the general procedure for the preparation of V using method A. 0.25 g (0.90 mmol) of 4-methoxy-4-oxo-3-(4-(trifluoromethyl) phenyl)butanoic acid afforded 0.193 g (46.8%) of compound 9 as light yellow solid. Mp

140–144 °C. ESI-MS m/z [M + H] \* = 456. ¹H NMR (300 MHz, CDCl<sub>3</sub>)  $\delta$  7.74 (d, J = 6.0 Hz, 2H), 7.69 (d, J = 9.0 Hz, 2H), 7.49–7.56 (m, 5H), 7.42 (d, J = 6.0 Hz, 2H), 7.36 (d, J = 9.0 Hz, 2H), 4.27 (dd, J = 10.6, 4.5 Hz, 1H), 3.64 (s, 3H), 3.21 (dd, J = 15.0, 9.0 Hz, 1H), 2.67 (dd, J = 15.0, 3.0 Hz, 1H). HRMS (ESI) m/z calculated for  $C_{25}H_{20}F_{3}NO_{4}$ : 455.1344, found [M + H] \* 456.1425.

methyl 4-((1-benzyl-1H-pyrazol-3-yl)amino)-4-oxo-2-(4-{triflu oromethyl)phenyl)butanoate (10). Compound 10 was prepared according to the general procedure for the preparation of V using method A. 0.25 g (0.90 mmol) of 4-methoxy-4-oxo-3-(4-(trifluoromethyl) phenyl)butanoic acid afforded 0.146 g (37.4%) of compound 10 as white solid. Mp 116–120 °C. ESI-MS m/z [M + 23] = 454.  $^1$ H NMR (300 MHz, Methanol- $^4$ )  $\delta$  7.65 (d,  $^4$ J = 9.0 Hz, 2H), 7.54 (m, 3H), 7.28–7.36

(m, 3H), 7.21 (d, J = 9.0 Hz, 2H), 6.51 (bs, 1H), 5.23 (s, 2H), 4.3 (dd, J = 12.0, 6.0 Hz, 1H), 3.69 (s, 3H), 3.25 (dd, J = 16.5, 10.5 Hz, 1H), 2.82 (dd, J = 16.5, 4.5 Hz, 1H). HRMS (ESI) m/z calculated for  $C_{22}H_{20}F_3N_3O_3$ : 431.1457, found [M + H]<sup>+</sup> 432.1537. **methyl 4-((4-(oxazol-2-yl)phenyl)amino)-4-oxo-2-(4-(trifluoro methyl)phenyl)butanoate** (11). Compound 11 was prepared according to the general procedure for the preparation of V using method A. 0.25 g of 4-methoxy-4-oxo-3-(4-(trifluoromethyl) phenyl)butanoic acid (0.90 mmol) afforded 0.343 g (90.7%) of compound 11 as white solid. Mp 214–216 °C. ESI-

MS m/z [M + H]<sup>+</sup> = 419. <sup>1</sup>H NMR (300 MHz, Methanol- $d_4$ )  $\delta$  7.95–7.98 (m, 3H), 7.66–7.71 (m, 4H), 7.56 (d, J = 9.0 Hz, 2H), 7.29 (bs, 1H), 4.34 (dd, J = 12.0, 6.0 Hz, 1H), 3.71 (s, 3H), 3.29 (m, 1H), 2.86 (dd, J = 15.0, 6.0 Hz, 1H). HRMS (ESI) m/z calculated for  $C_{21}H_{17}F_3N_2O_4$ : 418.1140, found [M + H]<sup>+</sup>419.1221. methyl 4-oxo-4-((4-(thiophen-2-yl)phenyl)amino)-2-(4-(tri-

**fluoromethyl)phenyl)butanoate** (12). Compound 12 was prepared according to the general procedure for the preparation of V using method A. 0.25 g (0.90 mmol) of 4-methoxy-4-oxo-3-(4-(trifluoromethyl) phenyl)butanoic acid afforded 0.26 g (66.3%) of compound

as yellow solid. Mp 201–205 °C. ESI-MS m/z [M + 23] = 456. ¹H NMR (300 MHz, CDCl<sub>3</sub>)  $\delta$  7.55–7.63 (m, 4H), 7.39–7.50 (m, 5H), 7.25 (d, J = 6.0 Hz, 1H), 7.07 (t, J = 4.5 Hz, 1H), 4.35 (dd, J = 10.5, 4.5 Hz, 1H), 3.71 (s, 3H), 3.25 (dd, J = 15.0, 12.0 Hz, 1H), 2.71 (dd, J = 4.5, 16.5 Hz, 1H). HRMS (ESI) m/z calculated for C<sub>22</sub>H<sub>18</sub>F<sub>3</sub>NO<sub>3</sub>S: 433.0959, found [M + H]\* 434.1037. **methyl 4-((4-(indoline-1-carbonyl)phenyl)amino)-4-oxo-2-(4-** (trifluoromethyl)phenyl)butanoate (13). Compound 13 was prepared according to the general procedure for the preparation of **V** using method A. 0.25 g (0.90 mmol) of 4-methoxy-4-oxo-3-(4-(trifluoromethyl) phenyl)butanoic acid afforded 0.13 g (28.9%) of compound

as white solid. Mp 218–222 °C. ESI-MS m/z [M + H]\* = 497. ¹H NMR (300 MHz, DMSO- $d_6$ )  $\delta$  10.28 (s, 1H), 7.74 (d, J = 6.0 Hz, 2H), 7.52–7.64 (m, 7 H), 7.26 (d, J = 6.0 Hz, 1H), 7.14 (t, J = 6.0 Hz, 1H), 7.01 (t, J = 6.0 Hz, 1H), 4.29 (dd, J = 9.0, 6.0 Hz, 1H), 4.03 (t, J = 7.5 Hz, 2H), 3.62 (s, 3H), 3.20 (dd, J = 18.0, 9.0 Hz, 1H), 3.07 (t, J = 9.0 Hz, 2H), 2.86 (dd, J = 15.0, 6.0 Hz, 1H). HRMS (ESI) m/z calculated for  $C_{27}H_{23}F_3N_2O_4$ : 496.1610, found [M + H]\* 497.1689. methyl 4-((4-(1H-tetrazol-5-yl)phenyl)amino)-4-oxo-2-(4-(trifluoromethyl)phenyl)butanoate (14). Compound 14 was prepared according to the general procedure for the preparation of  $\bf V$  using method A. 0.25 g (0.90 mmol) of 4-methoxy-4-oxo-3-(4-(trifluoromethyl) phenyl)butanoic acid afforded 0.15 g (39.5%) of compound

as light yellow solid. Mp 197–201 °C. ESI-MS m/z [M - H]\*  $\pm$  418. 
<sup>1</sup>H NMR (300 MHz, Methanol- $d_4$ )  $\delta$  7.94 (d, J = 6.0 Hz, 2H), 7.74 (d, J = 9.0 Hz, 2H), 7.64 (d, J = 9.0 Hz, 2H), 7.53 (d, J = 9.0 Hz, 2H), 4.32 (dd, J = 9.0, 6.0 Hz, 1H), 3.69 (s, 3H), 3.28 (dd, J = 15.0, 9.0 Hz, 1H), 2.82–2.91 (m, 1H). HRMS (ESI) m/z calculated for  $C_1$ 9H $_1$ 6F $_3$ N $_5$ O $_3$ : 419.1205, found [M + H]\* 420.1288. methyl 4-((4-(4-methylpiperazin-1-yl)phenyl)amino)-4-oxo-2- (4-(trifluoromethyl)phenyl)butanoate (15). Compound 15 was prepared according to the general procedure for the preparation of V using method A. 0.25 g (0.90 mmol) of 4-methoxy-4-oxo-3-(4-(trifluoromethyl) phenyl)butanoic acid afforded 0.10 g (24.6%) of compound 15 as white solid. Mp 248–252 °C.

ESI-MS m/z [M - H]<sup>+</sup> = 448.  $^{1}$ H NMR (300 MHz, Methanol- $d_{4}$ )  $\delta$  7.64 (d, J = 9.0 Hz, 2H), 7.52 (d, J = 9.0 Hz,

2H), 7.33 (d, J = 9.0 Hz, 2H), 6.91 (d, J = 9.0 Hz, 2H), 4.28 (dd, J = 10.5, 4.5 Hz, 1H), 3.68 (s, 3H), 3.21 (dd, J = 15.0, 9.0 Hz, 1H), 3.15 (m, 4H), 2.78 (dd, J = 16.5, 4.5 Hz, 1H), 2.59–2.62 (m, 4H), 2.34 (s, 3H). HRMS (ESI) m/z calculated for  $C_{23}H_{26}F_{3}N_{3}O_{3}$ : 449.1926, found [M + H]\* 450.2005.

methyl 4-((3-chloro-4-morpholinophenyl)amino)-4-oxo-2-(4-(trifluoromethyl)phenyl)butanoate (16). Compound 16 was prepared according to the general procedure for the preparation of V using method A. 0.25 g (0.90 mmol) of 4-methoxy-4-oxo-3-(4-(trifluoromethyl) phenyl)butanoic acid afforded 0.24 g (56.4%) of compound

**16** as light yellow solid. Mp 96–99 °C. ESI-MS m/z [M - H]\*  $_{=}$  469.  $^{1}$ H NMR (300 MHz, CDCl $_{3}$ )  $\delta$  7.56–7.61 (m, 3H), 7.41 (d, J = 9.0 Hz, 2H), 7.30 (s, 1H), 6.96 (d, J = 9.0 Hz, 1H), 4.31 (dd, J = 9.0, 6.0 Hz, 1H), 3.86

(t, J = 4.5 Hz, 4H), 3.7 (s, 3H), 3.2 (dd, J = 15.0, 9.0 Hz, 1H), 3.0 (t, J = 4.5 Hz, 4H), 2.67 (dd, J = 15.0, 6.0 Hz, 1H). HRMS (ESI) m/z calculated for  $C_{22}H_{22}CIF_3N_2O_4$ : 470.1220, found [M + H]\* 471.1295.

methyl 2-(4-methoxyphenyl)-4-((4-(1-methyl-1H-imidazole-2-carbonyl)phenyl)amino)-4-oxobutanoate (17). Compound 17 was prepared according to the general procedure for the preparation of V using method A. 0.265 g (1.11 mol) of 4-methoxy-3-(4-methoxyphenyl)- 4-oxobutanoic acid afforded 0.1 g (24.7%) of compound 17 as yellow solid. Mp 153–156 °C. ESI-MS

m/z [M – H]<sup>+</sup> = 420. <sup>1</sup>H NMR (300 MHz, DMSO- $d_6$ )  $\delta$  8.13 (d, J = 9.0 Hz, 2H), 7.70 (d, J = 9.0 Hz, 2H), 7.42 (s, 1H), 7.26 (d, J = 9.0 Hz, 2H), 7.18 (s, 1H), 6.90 (d, J = 9.0 Hz, 2H), 4.15

(dd, J = 10.6, 4.5 Hz, 1H), 4.05 (s, 3H), 3.79 (s, 3H), 3.68 (s, 3H), 3.25 (dd, J = 15.0, 9.0 Hz, 1H), 2.79 (dd, J = 16.5, 4.5 Hz, 1H). HRMS (ESI) m/z calculated for  $C_{23}H_{23}N_3O_5$ : 421.1638, found [M + H] $^+$ 422.1714.

methyl 4-((4-(1-methyl-1H-imidazole-2-carbonyl)phenyl) amino)-4-oxo-2-phenylbutanoate (18). Compound 18 was prepared according to the general procedure for the preparation of V using method A. 0.2 g (0.96 mmol) of 4-methoxy-4-oxo-3-phenylbutanoic acid afforded 0.162 g (57.2%) of compound

**18** as yellow solid. Mp 159–162 °C °C. ESI-MS m/z [M + H]\*  $_{\pm}$  392.  $^{1}$ H NMR (300 MHz,

DMSO- $d_6$ )  $\delta$  10.39 (s, 1H), 8.26 (d, J = 9.0 Hz, 2H), 7.68 (d, J = 9.0 Hz, 2H), 7.56 (s, 1H), 7.27–7.39 (m, 5H), 7.18 (s, 1H), 4.15 (dd, J = 10.6, 4.5 Hz, 1H), 3.97 (s, 3H), 3.59 (s, 3H), 3.20 (dd, J = 15.0, 9.0 Hz, 1H), 2.81 (dd, J = 16.5, 4.5 Hz, 1H). HRMS (ESI) m/z calculated for  $C_{22}H_{21}N_3O_4$ : 391.1532, found [M + H]+ 392.1609.

methyl 2-(4-fluorophenyl)-4-((4-(1-methyl-1H-imidazole-2-carbonyl)phenyl)amino)-4-oxobutanoate (19). Compound 19 was prepared

according to the general procedure for the preparation of **V** using method B. 0.4 g (1.76 mmol) of compound **4f** gave 0.25 g (42.2%) of compound **19** as yellow solid. Mp 183–185 °C. ESI-MS m/z [M + H]<sup>+</sup> = 410. (300 MHz, Methanol- $d_4$ )  $\delta$  ppm 8.13 (d, J = 9.0 Hz, 2 H), 7.70 (d, J = 9.0 Hz, 2 H), 7.42 (s, 1H), 7.35–7.40 (m, 2H), 7.19 (s, 1H), 7.09 (t, J = 9.0 Hz, 2H), 4.22 (dd, J = 10.6, 4.5 Hz, 1H), 4.05 (s, 3H), 3.69 (s, 3H), 3.26 (dd, J = 15.0, 9.0 Hz, 1H), 2.81 (dd, J = 15.0, 6.0 Hz, 1H). HRMS

(ESI) m/z calculated for  $C_{22}H_{20}FN_3O_4$ : 409.1438, found [M + H]+ 410.1515. HPLC purity determined using HPLC method 2 was 91.75%.

# 2-(4-chlorophenyl)-4-((4-(1-methyl-1H-imidazole-2-carbonyl)

phenyl)amino)-4-oxobutanoic acid (20). Compound 20 was prepared according to the general procedure for the preparation of VI. 50 mg (0.117 mmol) of compound 5, methyl 2-(4-chlorophenyl)-4-((4-(1- methyl-1H-imidazole-2-carbonyl)phenyl)amino)-4-oxobutanoate, afforded 26 mg (54.16 %) of compound 20 as light yellow solid. Mp

120–124 °C. ESI-MS m/z [M - H]\*  $\pm$  410.  $^1$ H NMR (300 MHz, Methanol- $d_4$ )  $\delta$  8.12 (d, J  $\pm$  9.0 Hz, 2H), 7.71 (d, J  $\pm$  7.5 Hz, 2H), 7.34–7.45 (m, 5H), 7.17 (s, 1H), 4.19 (dd, J  $\pm$  9.0, 6.0 Hz, 1H), 4.03 (s, 3H), 3.20–3.29 (m, 1H), 2.64–2.83 (m, 1H). HRMS (ESI) m/z calculated for C<sub>21</sub>H<sub>18</sub>CIN<sub>3</sub>O<sub>4</sub>: 411.0986, found [M + H]\* 412.1075.

anol- $d_4$ )  $\delta$  8.12 (d, J = 6.0 Hz, 2H), 7.57–7.75 (m, 6H), 7.40 (s, 1H), 7.11 (s, 1H), 4.28–4.32 (m, 1H), 4.03 (s, 3H), 3.35–3.30 (m, 1H), 2.71–2.86 (m, 1H).  $^{13}$ C NMR (75 MHz, Methanol-d4)  $\delta$  182.81, 143.31, 143.17, 132.23, 132.11, 131.68, 128.43, 128.19, 127.94, 126.97, 125.30, 118.35, 118.20, 48.47, 46.77, 34.96. HRMS (ESI) m/z calculated for  $C_{22}H_{18}F_3N_3O_4$ : 445.1249, found [M + H]\* 446.1348.

# 4-((3-fluoro-4-morpholinophenyl)amino)-4-oxo-2-(4-

(trifluoromethyl)phenyl)butanoic acid (22). Compound 22 was prepared according to the general procedure for the preparation of VI. 67 mg (0.147 mmol) of compound 7, methyl 4-((3-fluoro-4-morpholinophenyl)amino)-4-oxo-2-(4-(trifluoromethyl)phenyl)butanoate, afforded 24 mg (36.9%) of compound

**22** as white solid. Mp 180–183 °C. ESI-MS m/z [M + H]<sup>+</sup> = 441. <sup>1</sup>H NMR (300 MHz, Methanol- $d_4$ )  $\delta$  7.49–7.64 (m, 4H), 7.44 (t, J = 12.0 Hz, 1H), 7.16 (t, J = 10.5 Hz, 1H), 6.97 (t, J = 9.0 Hz, 1H), 4.24–4.26 (m, 1H), 3.83 (bs, 4H), 3.22–3.25 (m, 1H), 2.99 (bs, 4H), 2.72–2.76 (m, 1H). HRMS (ESI) m/z calculated for  $C_{21}H_{20}F_4N_2O_4$ :

440.1359, found [M + H]+441.1432.

 $H]^{+} = 446. \, ^{1}H \, NMR \, (300 \, MHz, \, Meth-$ 

# 4-((4-benzoylphenyl)amino)-4-oxo-2-(4-(trifluoromethyl)

**phenyl)butanoic acid (23).** Compound **23** was prepared according to the general procedure for the preparation of **VI.** 0.154 g (0.348 mmol) of compound **9**, methyl 4-((4-benzoylphenyl)amino)-4-oxo-2-(4-(trifluoromethyl)phenyl)butanoate, resulted in 97 mg (65.1%) of compound **23** as white solid. Mp 110–113 °C. ESI-MS m/z [M - H] $^+$  = 440.  $^1$ H NMR (300 Hz, Methanol- $d_4$ )  $\delta$  7.73–7.80 (m, 6H), 7.51–7.70 (m, 7H), 4.30 (dd, J = 10.5, 4.5 Hz, 1H), 3.28 (dd, J = 18.0, 9.0 Hz, 1H), 2.79 (ddd, J = 33.0, 18.0, 6.0 Hz, 1H). HRMS

(ESI) m/z calculated for  $C_{24}H_{18}F_3NO_4$ : 441.1188, found  $[M + H]^+$  442.1264.

# 4-oxo-4-((4-(thiophen-2-yl)phenyl)amino)-2-(4-

(trifluoromethyl)phenyl)butanoic acid (24). Compound 24 was prepared according to the general procedure for the preparation of VI. 0.14 g (0.322 mmol) of compound 12, methyl 4-oxo-4-((4-(thiophen-2-yl) phenyl)amino)-2-(4-(trifluoromethyl)phenyl)butanoate, afforded 81 mg (60%) of compound 24 as light yellow solid. Mp 256–259 °C. ESI-MS m/z [M - H]+ = 418. ¹H NMR (300 Hz, Methanol- $d_4$ )  $\delta$  7.61–7.66 (m, 3 H), 7.51–7.58 (m, 5H), 7.30 (d, J = 3.0 Hz,

2H), 7.05 (t, J = 4.5 Hz, 1H), 4.25 (dd, J = 10.5, 4.5 Hz, 1H), 3.24 (dd, J = 18.0, 9.0

Hz, 1H), 2.75 (td, J = 19.5, 6.0 Hz, 1H). HRMS (ESI) m/z calculated for  $C_{21}H_{16}F_3NO_3S$ :

419.0803, found [M + H]+420.0889.

# 4-((4-(1H-tetrazol-5-yl)phenyl)amino)-4-oxo-2-(4-

(trifluoromethyl)phenyl)butanoic acid (25). Compound 25 was prepared according to the general procedure for the preparation of VI. 0.12 g (0.286 mmol) of compound 14, methyl 4-((4-(1H-tetrazol-5-yl) phenyl)amino)-4-oxo-2-(4-(trifluoromethyl)phenyl)butanoate, afforded 61 mg of product (52.5%) as yellow solid. Mp 200–204 °C. ESI-MS m/z [M - H] $^+$  = 404.  $^1$ H NMR (300 Hz, Methanol- $^4$ d)  $\delta$  7.94 (d, J = 9.0 Hz, 2H), 7.72 (d, J = 9.0 Hz, 2H), 7.55–7.65 (m, 4H), 4.27 (dd, J = 9.0, 6.0 Hz, 1H), 3.22–3.33 (m, 1 H), 2.69–2.75 (m, 1H). HRMS (ESI) m/z calculated for  $C_{18}H_{14}F_3N_5O_3$ : 405.1049, found [M + H] $^+$  406.1130.

# 4-((3-chloro-4-morpholinophenyl)amino)-4-oxo-2-(4-

(trifluoromethyl)phenyl)butanoic acid (26). Compound 26 was prepared according to the general procedure for the preparation of VI. 0.125 g (0.265 mmol) of compound 16, methyl 4-((3-chloro-4-morpholinophenyl)amino)-4-oxo-2-(4-(trifluoromethyl)phenyl)butanoate afforded 90 mg (74.3%) of compound 26 as off-white solid. Mp 200–204 °C. ESI-MS m/z [M - H] $^+$   $\pm$  456.  $^1$ H NMR (300 Hz, Methanol-  $d_4$ )  $\delta$  7.54–7.70 (m, 5 H), 7.31–7.39 (m, 1H), 7.04 (d, J = 9 Hz, 1H),

4.10–4.24 (m, 1H), 3.81 (bs, 4H), 3.11–3.19 (m, 1H), 2.98 (bs, 4H), 2.61–2.76 (m, 1H). HRMS (ESI) m/z calculated for  $C_{21}H_{20}CIF_3N_2O_4$ : 456.1064, found [M + H] $^+$ 457.1145.

# 2-(4-methoxyphenyl)-4-((4-(1-methyl-1H-imidazole-2-

**carbonyl)phenyl)amino)-4-oxobutanoic acid (27).** Compound **27** was prepared according to the general procedure for the preparation of **VI.** methyl 2-(4-methoxyphenyl)-4-((4-(1-methyl-1H-imidazole-2-carbonyl)phenyl)amino)-4-oxobutanoate, compound **17**, 65 mg (0.154 mmol) afforded 25 mg (39.8%) of compound **27** as yellow solid. Mp 160–163 °C. ESI-MS m/z [M - H] $^+$  = 406.  $^1$ H NMR (300 Hz, Methanol-  $d_4$ )  $\delta$  8.00 (d, J = 9.0 Hz, 2H), 7.60 (t, J = 7.5 Hz, 2H), 7.29 (bs, 1H), 7.16–7.24 (m, 2H), 7.05 (bs, 1H), 6.78 (d, J = 9.0 Hz, 2H). 3.97–4.05 (m,

1H), 3.91 (s, 3H), 3.67 (s, 3H), 3.06–3.16 (m, 1H), 2.58 (ddd, J = 36.0, 15.0, 6.0 Hz, 1H). HRMS (ESI) m/z calculated for  $C_{22}H_{21}N_3O_5$ : 407.1481, found [M + H]\* 408.1560.

**4-((4-(1-methyl-1H-imidazole-2-carbonyl)phenyl)amino)-4- oxo-2-(2-phenylthiazol-4-yl)butanoic acid (28).** First, methyl 4-((4- (1-methyl-1H-imidazole-2-carbonyl)phenyl)amino)-4-oxo-2-(2-phenylthiazol-4-yl)butanoate was prepared according to the general procedure for the preparation of **V** using intermediate **4d.** Next, using the general procedure for the preparation of **VI**, we obtained 10 mg (22.9%) of compound **28** as yellow solid from 45 mg (0.094 mmol) of 4-((4-(1- methyl-1H-imidazole-2-carbonyl)phenyl)amino)-4-oxo-2-(2-phenylthiazol-4-yl)butanoate. ESI-MS m/z [M - H] $^+$  = 459.  $^1$ H NMR (300 Hz, Methanol- $d_4$ ) δ 8.14 (d, J = 9.0 Hz, 2H), 7.95–7.99 (m, 2H), 7.78 (d, J = 9.0 Hz, 2H), 7.41–7.48 (m, 5H), 7.17 (s, 1H), 4.51–4.56 (m, 1H), 3.20–3.30 (m, 1H), 2.94–2.99 (m, 1H). HRMS (ESI) m/z calculated for  $C_{24}H_{20}N_4O_4S$ : 460.1205, found [M + H] $^+$  461.1281.

# 4.1.6. Synthesis of amino-3-(3-chlorophenyl)propanoic acid (30)

2.74 (m, 2 H).

3-chloro benzaldehyde (**29**) (4.03 mL, 35.56 mmol, 1 equiv) was dissolved in ethanol (90 mL) and malonic acid (3.7 g, 35.5 mmol, 1 equiv) and ammonium acetate (5.48 g, 71.09 mmol, 2 equiv) were added to the reaction mixture. The reaction was heated to reflux for 4 h. After the reaction, the reaction mixture was filtered and the solid obtained was dried in vacuum. The crude obtained was purified using flash chromatography to give 3.4 g (47.9%) of **30** as orange color solid. ESI- MS m/z [M - H]<sup>+</sup> = 198. <sup>1</sup>H NMR (300 Hz, Methanol- $d_4$ )  $\delta$  7.54 (s, 1H), 7.41–7.45 (m, 3 H), 4.55 (t, J = 12 Hz, 1 H), 2.70–

4.1.7. Synthesis of ethyl 3-amino-3-(3-chlorophenyl)propanoate (31) amino-3-(3-chlorophenyl)propanoic acid (0.7 g, 3.5 mmol, 1 equiv) was added to a solution of thionyl chloride (0.382 mL, 5.26 mmol, 1.5 equiv) in ethanol at 0 °C.

The reaction was allowed to come to room temperature and heated to 65 °C for 6 h. The reaction mixture was treated with aq. NaHCO<sub>3</sub> and extracted with EtOAc. The organic layer was dried over Na<sub>2</sub>SO<sub>4</sub> and evaporated in vacuo. The crude was purified using flash chromatography to give 0.65 g (81.3%) of compound **31** as white solid. ESI-MS m/z [M + 23] = 249. <sup>1</sup>H NMR (300 Hz, CDCl<sub>3</sub>)  $\delta$  7.30 (s, 1H), 7.13–7.21 (m, 3H), 4.32 (t, J = 6.0 Hz, 1H), 4.06 (q, J = 7.0 Hz, 2H), 2.55 (d, J = 6.0 Hz, 2H), 1.15 (t, J = 7.5 Hz, 3H).

# 4.1.8. Synthesis of ethyl 3-(2-chlorobenzamido)-3-(3-chlorophenyl) propanoate (32a)

Pyridine (0.159 mL, 1.99 mmol, 3 equiv) was added to a reaction mixture containing ethyl 3-amino-3-(3-chlorophenyl)propanoate (31) (0.15 g, 0.659 mmol, 1 equiv) in THF (12 mL) and DMF (2.4 mL). 2- chloro benzoylchloride (0.108 mL, 0.856 mmol, 1.3 equiv) was then added and the reaction stirred at rt for 24 h. After the reaction, the reaction was acidified by 1% HCl and extracted with DCM. The organic layer was separated, dried over Na<sub>2</sub>SO<sub>4</sub> and evaporated in vacuo. The compound was purified using flash chromatography to give 0.2 g (84.3%) of compound 32a as white solid. ESI-MS m/z [M - H] $^+$  = 364.  $^1$ H NMR (300 Hz, CDCl<sub>3</sub>)  $\delta$  7.65 (d, J = 6.0 Hz, 1H), 7.49 (d, J = 9.0 Hz, 1H), 7.25-7.39 (m, 6H), 5.61 (q, J = 7.0 Hz, 1H), 4.09 (q, J = 7.0 Hz, 2H), 2.96 (t, J = 7.0 Hz, 2H), 1.18 (t, J = 7.0 Hz, 3H).

4.1.9. Synthesis of intermediates **31b-31d**. Intermediates **32b-32d** were synthesized utilizing Method B, as outlined in the general procedure for the preparation of compound  ${\bf V}$ 

ethyl 3-(3-chlorophenyl)-3-(3-phenylpropanamido)propanoate (32b). 3-phenylpropionic acid (0.132 g, 0.879 mmol) was reacted with ethyl 3-amino-3-(3-chlorophenyl)propanoate (31) (0.2 g, 0.87 mmol) to give 0.26 g (82.2%) of

compound **32b** as white solid. ESI-MS m/z [M - H]<sup>+</sup> = 358. <sup>1</sup>H NMR (300 Hz, CDCl<sub>3</sub>)  $\delta$  7.29-7.31 (m, 1H), 7.20-7.23 (m, 4H), 7.18 (d, J = 6.0 Hz, 2H), 7.03 (t, J = 4.5 Hz, 1H), 6.57 (d, J = 6.0

Hz, 1H), 5.28 (q, J = 6.0 Hz, 1H), 4.05 (q, J = 7.0 Hz, 2H), 2.99 (t, J = 7.5 Hz, 2H), 2.82 (dd, J = 15.0, 6.0 Hz, 1H), 2.69 (dd, J = 15.0, 6.0 Hz, 1H), 2.56 (t, J = 7.5 Hz, 2H), 1.17 (t, J = 7.5 Hz, 3H).

ethyl 3-(3-chlorophenyl)-3-(2-phenylacetamido)propanoate (32c). phenylacetic acid (0.15 g, 1.10 mmol) was reacted with ethyl 3- amino-3-(3-chlorophenyl)propanoate (31) (0.25 g, 1.09 mmol) to give 0.355 g (93.4%) of compound 32c as white solid. ESI-MS m/z [M - H] $^+$  = 344.  $^1$ H NMR (300 Hz, CDCl $_3$ )  $\delta$  7.28 (d, J = 6.0 Hz, 1H), 7.23 (d, J =

6.0 Hz, 1H), 7.19 (t, J = 6.0 Hz, 3H), 7.10 (d, J = 6.0 Hz, 2H), 7.06 (s, 1H), 6.96 (t, J = 4.5 Hz, 1H), 6.77 (d, J = 6.0 Hz, 1H), 5.27 (q, J = 7.0 Hz, 1 H), 3.90 (q, J = 7.0 Hz, 2H), 3.48 (s, 2H), 2.64 (t, J = 4.5 Hz, 2H), 1.01 (t, J = 7.5 Hz, 3H). **ethyl 3-(3-chlorophenyl)-3-(2-(4-(trifluoromethyl)phenyl)acet-**

**amido)propanoate (32d).** 2-(4-(trifluoromethyl)phenyl)acetic acid (0.224 g, 1.09 mmol) was reacted with ethyl 3-amino-3-(3-chlorophenyl)propanoate (31) (0.25 g, 1.09 mmol) to give 0.3 g (66.07%) of compound 32d as white solid.

ESI-MS m/z [M - H]\* = 412. <sup>1</sup>H NMR (300 Hz, CDCl<sub>3</sub>)  $\delta$  7.53 (d, J = 6.0 Hz, 2 H), 7.42 (d, J = 9.0 Hz, 1 H), 7.32 (d, J = 9.0 Hz, 2H), 7.14–7.18 (m, 2H), 7.05–7.08 (m, 1H), 5.36 (q, J = 7.0 Hz, 1H), 4.00 (q, J = 8.0, 2H), 3.51 (s, 2H), 2.72 (t, J = 6.0 Hz, 2H), 1.10 (t, J = 7.5 Hz, 3 H).

4.1.10. Synthesis of compounds **33–36**.The ethyl esters of intermediates **32a-32d** were hydrolyzed using the general procedure for the preparation of **VIII** 

**3-(2-chlorobenzamido)-3-(3-chlorophenyl)propanoic acid (33)**. Compound **32a**, Ethyl 3-(2-chlorobenzamido)-3-(3-chlorophenyl)propanoate (0.25 g, 0.682 mmol) after reaction afforded 0.115 g (49.7%) of compound **33** as white solid.

Mp 146–147 °C. ESI-MS m/z [M + H]<sup>+</sup> = 338. ¹H NMR (300 Hz, Methanol- $d_4$ )  $\delta$  7.50 (s, 1H), 7.37–7.46 (m, 6H), 7.32 (t, J = 6.0 Hz, 1H), 5.55 (t, J = 7.5 Hz, 1H), 2.90 (dd, J = 9.0, 3.0 Hz, 2H). HRMS (ESI) m/z calculated for  $C_{16}H_{13}Cl_2NO_3$ : 337.0272, found [M + H]<sup>+</sup>338.0354.

**3-(3-chlorophenyl)-3-(3-phenylpropanamido)propanoic acid (34).**Compound **32b, 3** ethyl 3-(3-chlorophenyl)-3-(3-

7.5 Hz, 1H), 2.90 (t, J = 7.5 Hz, 2H), 2.74 (d, J = 6.0 Hz, 2H), 2.52 (t, J = 7.5 Hz, 2H). HRMS (ESI) m/z calculated for  $C_{18}H_{18}CINO_3$ : 331.0975, found [M + H]\* 332.1053.

**3-(3-chlorophenyl)-3-(2-phenylacetamido)propanoic** acid (35). Compound **32c**, ethyl 3-(3-chlorophenyl)-3-(2-phenylacetamido)propanoate (0.33 g, 0.954 mmol) afforded 0.1 g (33.0%) of compound **35** as white solid. Mp 121–122 °C. ESI-MS m/z [M + H] $^+$  = 318  $^1$ H NMR (300 Hz, Methanol- $d_4$ ), 7.34 (s, 1H), 7.22–7.30 (m, 8H), 5.30 (t, J = 6.0 Hz, 1H), 3.55 (s, 2H), 2.82 (dd, J = 6.0, 3.0 Hz, 2H). HRMS (ESI) m/z calculated for  $C_{17}H_{16}CINO_3$ : 317.0819, found [M + H] $^+$  318.0898.

**3-(3-chlorophenyl)-3-(2-(4-(trifluoromethyl)phenyl)acetamido) propanoic acid (36).** Compound **32d,** ethyl 3-(3-chlorophenyl)-3-(2- (4-(trifluoromethyl)phenyl)acetamido)propanoate (0.285 g, 0.688 mmol), afforded 0.077 g (29.0%) of compound **36** as white solid. Mp 162–165 °C. ESI-

MS m/z [M + H]<sup>+</sup> = 386. <sup>1</sup>H NMR (300 Hz, Methanol-  $d_4$ ) 7.59 (d, J = 9.0 Hz, 2H), 7.45 (d, J = 9.0 Hz, 2H), 7.23–7.33 (m, 4H), 5.35 (t, J = 7.5 Hz, 1H), 3.63 (s, 2H), 2.81 (dd, J = 9.0, 3.0 Hz, 2H).

HRMS (ESI) m/z calculated for  $C_{18}H_{15}CIF_3NO_3$ : 385.0693, found [M + H]\* 386.0770.

# 4.2. Isolation of isomers of compound 21

# 4.2.1. Procedure for the separation of isomers by prep-HPLC

The study was performed by a CRO company VivaBiotech. The racemic mixture of compound **21** (1.07 g, 2.4 mmol) was separated by reverse phase HPLC on a C18 column eluting with acetonitrile/water (25%–95% with 10 mM NH<sub>4</sub>HCO<sub>3</sub>). The fractions were freeze-dried on lyophilizer to afford A1 (375 mg, 0.84 mmol, 35% yield) and A2 (440 mg, 0.99 mmol, 41 % yield) as white solids. The detailed chromatography method and analytical report are provided in the supplementary information.

A1: LCMS calc. for  $C_{22}H_{19}F_3N_3O_4$  [M+H]+: m/z = 446.1; Found: 446.1, rt = 1.508min

A2: LCMS calc. for  $C_{22}H_{19}F_3N_3O_4$  [M+H]+: m/z = 446.1; Found: 446.1, rt = 1.526min.

# 4.2.2. Procedure for the chiral separation of A1 by SFC

Fraction A1 (375 mg, 0.84 mmol) was subjected to chiral separation by SFC on a Daicel WHELK-3 column, and the A1P1 and A1P2 fractions were concentrated under reduced pressure. The residue was freeze-dried on lyophilizer to afford A1-P1 (150.15 mg, 0.34 mmol, 40% yield, 100% ee, rt = 1.211 min on WHELK column) and A1-P2 (128.01 mg, 0.29 mmol, 34% yield, 99% ee, rt = 1.456 min on WHELK column) as white solids. A1-P1 specific optical rotation [ $\alpha$ ] [25]<sub>D</sub> =  $_{+}$ 97.8° (c 0.3044, MeOH). LCMS calc. for C<sub>22</sub>H<sub>19</sub>F<sub>3</sub>N<sub>3</sub>O<sub>4</sub>

[M+H]\*: m/z = 446.1; Found: 446.1, rt = 1.564 min. A1-P2 [ $\alpha$ ] [25] $_D$  =  $_$  94.6° (c 0.3145, MeOH), LCMS calc. for  $C_{22}H_{19}F_3N_3O_4[M+H]^+$ : m/z = 446.1; Found: 446.1, rt = 1.566min. The chromatographic conditions are provided in the

# 4.2.3. Procedure for the chiral separation of A2 by SFC

supplementary information.

Fraction A2 (440 mg, 0.99 mmol) was subjected to chiral separation by SFC on an OD column, and the A2P1 and A2P2 fractions were concentrated under reduced pressure. The residue was freeze-dried on lyophilizer to afford A2P1 (179.64 mg, 0.40 mmol, 41 % yield, 99.5% ee, rt = 1.051 min on OD column) and A2P2 (180.97 mg, 0.41 mmol, 41% yield, 99.4% ee, rt = 1.405 min on OD

column) as white solids. A2P1, [ $\alpha$ ] [25]<sub>D</sub> =  $_{+}$ 145.6° (c 0.3171, MeOH), LCMS calc. for

 $C_{22}H_{19}F_3N_3O_4[M+H]^+$ : m/z = 446.1; Found: 446.1, rt = 1.588min. A2P2 [ $\alpha$ ] [25]<sub>D</sub>

 $= -135.8^{\circ}$  (c 0.3066, MeOH). LCMS calc. for

 $C_{22}H_{19}F_3N_3O_4$  [M+H]+: m/z = 446.1; Found: 446.1, rt = 1.585min. The chromatographic conditions are provided in the supplementary information.

### 4.3. Surface plasmon resonance binding assay

The binding affinity was calculated by SPR using the Biacore T200 instrument (Cytiva). His-tagged LDHA was immobilized on a CM5 sensor chip by standard amine-coupling. pH scouting was first performed to determine the appropriate pH for the amine coupling of protein to the chip surface. From scouting, pH 5.0 was chosen as the optimal pH for immobilization. The dextran matrix was activated with an injection of a mixture of 1-ethyl-3-(3-dimethylaminopropyl) carbodiimide and N-hydroxysuccinimide. The ligand was then passed over the activated surface to link the ligand to dextran. Finally, ethanolamine is passed over the sensor surface to deactivate any remaining esters. One flow cell of the CM5 chip is reserved as the control blank. R<sub>max</sub> is calculated from immobilized ligand levels. Calculated R<sub>max</sub> = (analyte MW/ligand MW) x immobilization amount x stoichiometric ratio). The final immobilized level for flow cell two (his-hLDHA) was 6454.2 RU, and for flow cell one (reference) was 143.6 RU. Compound solutions with increasing concentrations (0, 10  $\mu$ M, 50  $\mu$ M, 125  $\mu$ M, 250  $\mu$ M, and 500  $\mu$ M), in triplicate, were applied to all active and reference channels in SPR binding buffer (10 mM HEPES, pH 7.4, 150 mM NaCl, and 0.05% Tween-20, 0.5 mM TCEP, and 2% DMSO) at a 50 µL/min flow rate at 25 °C. Samples were injected for 30 s, and a 180-s dissociation phase was recorded. Sensograms were double referenced with a reference channel and zero concentration responses, and reference subtracted sensograms were fitted with a 1 to 1 Langmuir kinetic model producing two rate constants ( $K_a$  and  $K_d$ ), which were used to determine the equilibrium dissociation constants ( $K_D$ ). For steady-state affinity fittings, response units at each concentration were measured during the equilibration plateau phase, and the K<sub>D</sub> values were determined by fitting the data to a single rectangular hyperbolic curve equation.

# 4.4. Crystallization of compound 21

Single crystal X-ray diffraction analyses were carried out on a Bruker D8 Venture equipped with dual sealed tube MoK $\alpha$  ( $\lambda$  = 0.71073 Å) and CuK $\alpha$  ( $\lambda$  = 1.54178 Å) anodes operating at 50.0 kV and 1.40 mA (MoK $\alpha$ ) and 1.10 mA (CuK $\alpha$ ) and Helios multilayer X-ray optics.

# 4.4.1. Crystallization of A1P1 isomer of 21

One spatula (approximately  $5^{\sim}10$  mg) of A1P1 was dissolved in 1 mL of methanol in a 5 mL vial, followed by the addition of 5 drops of ethyl acetate. The vial was capped to permit solvent evaporation at room temperature. After 2 days, colorless crystals were obtained from a nearly dried solution.

# 4.4.2. Crystallization of A1P2 isomer of 21

One spatula (approximately  $5^{\sim}10$  mg) of LDI-A1P2 was dissolved with 1 mL of acetonitrile in a 5 mL vial, followed by the addition of 0.5 mL of diethyl ether. The vial was capped to permit solvent evaporation at room temperature. After 1 day, colorless crystals were obtained from a nearly dried solution.

# 4.4.3. Data Collection and refinement

The single crystals were mounted on MicroMesh (MiTeGen) cryoloops with immersion oil at 100 K under a nitrogen cryostream. A total of 29,664 and 29,709 reflections for A1P1 and A1P2, respectively, using (CuKα) were collected. Data were collected using 1° w and f-scans with 50–80 s exposures per frame using a PHOTON III C14 detector. Preliminary lattice constants and the intensities were integrated using the Bruker APEX4 program. The structures were determined by intrinsic phasing (SHELXT 2014/5) [37] and refined by full-matrix least-squares refinement on F2 (SHELXL-2017/1) [38] using the Olex2 software package using least-squares minimization. The final structural model incorporated anisotropic and isotropic atomic displacement parameters for non-hydrogen and hydrogen atoms, respectively. The hydrogen atoms attached to carbon atoms were eventually placed in calculated positions and refined in

the riding model sp2-or sp3-hybridized positions with C–H bond lengths of 0.95–0.99 Å. Relevant crystallographic and structure refinement data is provided in the supplementary information.

# 4.5. LDHA cloning and purification

A codon-optimized gBLOCK construct of human LDHA (Uniprot P00338) spanning residues A2 to F322 was purchased from Integrated DNA Technologies, Inc. The construct was inserted into a pTBSG vector [39], linearized at the Sspl site, using ligation-independent cloning. The final construct contained an N-terminal hexahistine tag and a tobacco etch virus protease (TEV) that provides the option of removal of the tag

(MHHHHHHSTSVDLGTENLYFQ/A) that would produce a protein spanning A2 to F322 of LDHA with no cloning artifacts remaining. The construct was transformed by heat shock into competent E. coli BL21 (DE3) pRARE cells that were grown on LB agar plates containing 50 μg/mL ampicillin and 34 μg/mL chloramphenicol. Seguences verified colonies were used to inoculate a culture in 10 mL starter culture in LB media that was added to 2 L of LB media and incubated at 37 °C until the OD<sub>600</sub> reached 0.6. Induction was carried out with the addition of 0.4 mM IPTG, and protein was expressed at 17 °C overnight. Cells were lysed by a freeze/thaw cycle and sonication, and the clarified lysate in buffer A (500 mM NaCl, 50 mM Tris pH 8.0) was applied to a 5 mL His-Trap nickel chelating column (Cytiva Life Sciences). The protein was eluted using a linear gradient from 10% to 50% buffer B (500 mM NaCl, 50 mM Tris pH 8.0, 500 mM imidazole) over 10 column volumes. Elution fractions were purified further by size exclusion chromatography with a Superdex 200 Increase column (Cytiva Life Sciences) equilibrated with 200 mM NaCl, 50 mM Tris-HCl pH 7.5. The LDHA fractions, consistent with a tetramer based on the column calibration standards, were pooled and concentrated to 11.9 mg/mL (0.31 mM). The total yield of purified LDHA was 7.7 mg.

# 4.6. Co-crystallization and data collection

Purified LDHA, containing the hexahistine tag, was used to prepare the complex with compound 21. A 100 mM stock solution of 21 was prepared in DMSO and added to an aliquot of the protein at a concentration of 2 mM. The complex was incubated on ice for 30 min prior to screening. All crystallization screening experiments were set up using an NT8 drop-setting robot (Formulatrix Inc.) and UVXPO MRC (Molecular Dimensions) sitting-drop vapor diffusion plates at 18 °C. 100 nL of protein and 100 nL crystallization solution were dispensed and equilibrated against 50  $\mu L$  of the latter. Initial crystals displaying a prismatic morphology were observed within approximately 10 days from the Index HT screen (Hampton Research) condition C9 (1.1 M sodium malonate, 0.1 M HEPES pH 7.0, 0.5%v/v Jeffamine ED-2001). These crystals belonged to an orthorhombic P form (LDHA:21-o). The crystallization conditions were subsequently refined using the Index C9 condition, and the best samples were obtained at pH 7.5 with all other components identical. These crystals adopted a primitive monoclinic form (LDHA:21-m). Samples were transferred to a cryoprotectant composed of 3.4 M sodium malonate pH 7.5, harvested, and stored in liquid nitrogen for X-ray diffraction data collection.

# 4.7. Co-crystal structure solution and refinement

X-ray diffraction data were collected at the National Synchrotron Light Source-II (NSLS-II) NYX beamline 19-ID using an Eiger2 XE 9 M pixel array detector. Intensities were integrated using XDS [40] via Autoproc [41] and the Laue class analysis, and data scaling were performed with Aimless [42]. Structure solution was conducted by molecular replacement with Phaser [43] using a previously determined LDHA structure (PDB 5W8J) as the search model. The top solution was obtained in the space group  $P2_1$  with four molecules in the asymmetric unit. Refinement and manual model building were conducted with Phenix [44] and Coot [45], respectively. Disordered side chains were truncated to the point for which electron density could be observed. Structure validation was conducted with Molprobity [46], and figures were prepared

using the CCP4MG package [47]. Superposition of structures was conducted using GESAMT [48] via the CCP4 [49] interface. Polder [50] omit maps were calculated with Phenix. Relevant crystallographic data are provided in supplementary information (Table S2).

# 4.8. In vitro LDHA/LDHB inhibition assay

The hLDH5 (LDHA) (Lee BioSolutions) inhibition assay was performed by measuring the fluorescence (excitation@340 nm, emission@460 nm) and monitoring the NADH conversion rate to NAD + at 37 °C [30]. The hLDH5 inhibition assays were carried out in 96-well plates with the following final enzyme and buffer concentration: 100 mM phosphate buffer (pH = 7.4), 0.003 units of LDHA, 40  $\mu$ M NADH (~2  $\times$  Km), and 1.44 mM pyruvate (saturated pyruvate conditions). The stock solution of compounds was prepared in dimethyl sulfoxide (DMSO). GNE-140 and DMSO were used as positive and negative controls, respectively. The experiment involved adding a solution of compounds in DMSO to the enzyme and NADH in a phosphate buffer. The assay plate was incubated at 25 °C for 10 min, and a baseline read was taken, after which pyruvate was added. The fluorescence was read for 5 min every 30 s in a BioTek Synergy HTX Multimode Reader. The slope of a suitable linear timeframe was calculated with the curve bottom assigned to the initial 5-s recording before adding pyruvate (background rate) and the curve top to the negative (DMSO only) control wells rate. Compounds were first tested at a single 100  $\mu M$  concentration, and a full dose response curve with 6–9 concentrations were prepared for compounds exhibiting ≥20% enzyme inhibition. IC<sub>50</sub> values were determined from dose-response curves using the four-parameter logistic nonlinear regression analysis (GraphPad Prism Software v9.0). Compounds exhibiting <20% inhibition were reported as IC<sub>50</sub> >100  $\mu$ M. The hLDH1 inhibitory activity of promising hits was determined using similar assay conditions with 0.0026 units of hLDH1, 1440  $\mu$ M pyruvate, and 40  $\mu$ M NADH (~2 × Km) concentrations. The assays were performed in triplicates (n = 3) and the data is presented as mean  $\pm$  SD.

# 4.9. Cell lines

PANC-1, MiaPaCa-2 and HPNE cell lines were obtained from the American Type Culture Collection (ATCC, Manassas, Virginia). FC1199 cells were obtained from Dr. David Tuveson, Cold Spring Harbor Laboratory. All cell lines were cultured in DMEM (Hyclone, DMEM/high glucose, Cat# SH30243.01 with the addition of 10% Cosmic Calf Serum) (GIBCO, DMEM/high glucose, DMEM Cat# 11995040 with 10% FBS) and Pen/Strep and maintained in a 37 °C, 5 % CO2/95% humidified air incubator.

# 4.10. Lactate accumulation assay

Lactate production in the medium was detected using the Lactate Assay Kit (catalog # K-607, BioVision, Mountain View, California). Specifically, MIAPaCa-2 cells were seeded in standard DMEM in a 6-well Nunclon plate at a density of  $4 \times 10^5$ /well and permitted to adhere overnight. The next day, the cells were washed with PBS and treated with compound or vehicle control (v/v%) for 6 h in a treatment media comprising DMEM with varied glucose and pyruvate concentrations and without serum and phenol red. At the end of 6 h, 2  $\mu L$  of culture medium was taken for the lactate assay and diluted 100-fold with the lactate assay buffer. The cells were collected and lysed, and the lysate was used for protein quantification. The lactic acid secreted in the medium was determined per the manufacturer's protocol, with fluorescence measured at  $E_x/E_m$  = 535/587 nm. A standard curve was used to quantitate the lactic acid in the culture medium. The OD values were normalized to the total protein. Experiments were performed in triplicate and repeated at least three times. The data were normalized to untreated cells (control), and the percent lactate production was calculated by using the equation (lactate in the control wells lactate in the experimental group)/control group  $\times$  100 %. Statistical analysis was conducted using Prism 9.0 software (GraphPad). Differences between the groups were explored by one-way analysis of variance (ANOVA) followed by

Dunnett's multiple comparison test. *P* value < 0.05 was considered significant. *4.11. Protein extraction* 

After 6 h of treatment with the inhibitors, the cells were gently scrapped and lysed using ice-cold RIPA buffer supplemented with protease inhibitors. The lysate was incubated (4  $^{\circ}$ C for 20 min) and then centrifuged (15,000g, 20 min, 4  $^{\circ}$ C) to collect the supernatant containing the total proteins. The total protein in cell lysates was then quantified using the BCA assay kit (catalog#23227).

# 4.12. Metabolomics assay

MIA PaCa-2 cells were treated with compound 21 (15  $\mu$ M) or untreated control for 6 h and 24 h, respectively. Cells were washed twice with PBS and gently scrapped before the pellet was obtained and stored at - 78 °C until analysis. The cell lysates were quantified by UPLC-MS to determine the intracellular levels of pyruvic acid, lactic acid, and twenty additional targeted acids, including TCA cycle metabolites. The study was performed by CRO, Creative Biosciences. Each cell sample (n = 3) was made to 250  $\mu$ L in 80% methanol. Cells were lysed on a MM 400 mill mixer at a shaking frequency of 30 Hz with the aid of two metal balls. The samples were subsequently sonicated for 1 min in an ice-water bath before centrifugal clarification at 21,000 g and 5 °C for 10 min. The clear supernatants were collected for the following assays. The protein pellets were used for protein assay using a standard BCA procedure and the concentration determined was normalized to the total amount of protein. A standard stock solution of 22 targeted organic acids was prepared at 100  $\mu M$  or 500  $\mu M$  concentration. This solution was serially diluted to make 10 calibration solutions. 40 µL of each calibration solution or 40 µL of the supernatant of each sample was mixed in turn with 40 μL of an internal standard solution of ten <sup>13</sup>C-labeled or deuterated organic acids, 80  $\mu$ L of 3-NPH solution, and 80  $\mu$ L of EDC-6% pyridine solution. The mixtures were allowed to react at 30  $^{\circ}$ C for 30 min. After reaction, 5  $\mu$ L of the resultant solutions were injected into a C18 column (2.1 × 150 mm, 1.8 um) to run LC-MRM/MS with negative ion detection on an Agilent 1290 UHPLC system coupled to an Agilent 6495B triple quadrupole MS instrument. Concentrations of the detected analytes were calculated with internal standard calibration by interpolating the constructed linear regression curves of individual compounds. Quantification analysis was performed for lactic acid, acetoacetic acid, acotinic acid, 2-hydroxyglutaric acid, 2-ketoglutaric acid, 3-hydroxybutyric acid, citric acid, ethylmalonic acid, fumaric acid, gluconic acid, glucuronic acid, glutaric acid, glyceric acid, glycolic acid, isocitric acid, itaconic acid, lactic acid, malic acid, malonic acid, methylmalonic acid, oxaloacetic acid, pyruvic acid, and succinic acid.

# 4.13. Extracellular flux analysis

Analyses of real-time extracellular acidification rate (ECAR) and oxygen consumption rate (OCR) for indicators of the two major energy- producing pathways, glycolysis, and oxidative phosphorylation, were performed using the Seahorse XFe96 Extracellular Flux Analyzer (Agilent Santa Clara, CA, USA). Briefly, MIA PaCa-2 cells cultured in DMEM medium comprising 10 mM glucose, 1 mM pyruvate, and 2 mM glutamine, were plated at 25,000 cells/well in XFp (Agilent) cell culture mini plates for 24 h at 37 °C. For the glycolytic rate assay, cells were treated with indicated concentrations of compound 21 or untreated control (DMSO) for 6 h, after which cells were washed and treated with XF media (XF DMEM pH 7.4 comprising 10 mM glucose, 1 mM pyruvate, and 2 mM glutamine). Cells were incubated for 1 h before the assay at 37 °C and washed with fresh XF media before the OCR and ECAR measurements according to the manufacturer's instructions. Three measurements of basal OCR or ECAR (18 min) were recorded before the injection of 0.5 µM Rotenone plus Antimycin A, following which another three measurement cycles were recorded. Subsequently, 2-deoxy-D- glucose (50 mM) was injected from port B, and the changes in OCR/ ECAR were measured for an additional five measurement cycles (30 min). For the ATP rate assay, MIA PaCa-2 cells were treated with the indicated concentration of compound **21** for 24 h, and real-time analysis was performed upon the addition of metabolic modulators, **1.5**  $\mu$ M oligomycin (port A) and 0.5  $\mu$ M of a mix of rotenone and antimycin A (port B)

# 4.14. ATP detection assay

MIA PaCa-2 cells were seeded at 10,000 cells/well for overnight in 96-well plates and treated with 10  $\mu$ M, 15  $\mu$ M, and 30  $\mu$ M of compound or untreated control for 48 h. Intracellular ATP levels were determined using CellTiter-Glo® 2.0 Assay according to the manufacturer's specification. 4.15. Antiproliferative assay

Pancreatic cancer cells were plated on a 96-well plate, and 1:2 serial dilution of compounds was done with 25 µM as the maximum dose for 2 h in serum-free media, and then 10 % serum was added for an additional 46 h. Compounds were prepared in DMSO, which did not exceed a maximum concentration of 0.2%. At the end of 48 h period, Hoechst 33342 (1.0  $\mu$ M) and SYTOX Green (0.5  $\mu$ M) fluorescent dyes were added to each well for 15 min. Confocal images were acquired using the Operetta High Content Imaging System (PerkinElmer). Five fields were screened in each well using a 10 × field objective with Hoechst 33342 detected using an excitation wavelength of 360-400 nm and an emission wavelength of 490-500 nm. SYTOX Green was detected using an excitation wavelength of 500-520 nm and an emission wavelength of 520-530 nm. Bright-field images were acquired for each field. Images were analyzed using Harmony software (PerkinElmer) with the cellpermeable vital dye Hoechst 33342 to identify cell nuclei (i.e., for cell counts). The normal cell impermeable SYTOX Green was used to identify necrotic cells. Cell counts were summed over the five fields for each well, and the percentage of viable cells was calculated relative to the untreated control. Linear regression dose-response (variable slope) analysis was used to calculate the concentration at which the drugs induce 50% cell death, an IC<sub>50</sub> value, for each extract using Prism Software version 9.0. Standard deviations are reported for IC<sub>50</sub> values representing >3 biological replicates (3 technical replicates/biological replicates) per compound.

4.16. MTS assay

MIA PaCa-2 cells at a density of  $1\times10^5$  cells/well or pancreatic cancer organoids were seeded to a 96-well clear, flat bottom microplate in 100  $\mu L$  complete culture medium and treated with the indicated concentration of compounds 6 and 21 for 48 h. At predetermined timepoints, 20  $\mu L$  of 3-(4,5-dimethylthiazol-2-yl)-5-(3-carboxymethoxyphenyl)-2-(4-sulfophenyl)-2H-tetrazolium (MTS) was added to each well. After 2–3 h of incubation, the absorbance at 490 nm was measured with BioTek Synergy HTX Multimode Reader using the medium-only control wells as blanks. The IC50 values were determined by comparing the absorbance in wells containing cells and test compounds to untreated cell control wells.

# 5. Statistical analysis

Statistical analysis was carried out by GraphPad Prism Software (version 9.0, GraphPad Software, San Diego, CA, USA). Biological studies were carried out in triplicates and were repeated three times. The data were processed using one-way analysis of variance (ANOVA) followed by Dunnett's multiple comparison test. Group differences were considered significant when  $p \le 0.05$ .

# Accession codes

The small molecule structures have been deposited to the Cambridge Structural Database (CSD) with the deposition numbers **21\_**A1P1 (2351470) and **21\_**A1P2 (2351471).

Coordinates and structure factors for the structure of LDHA in complex with compound **21** have been deposited to the Worldwide Protein Databank (wwPDB) with the accession code 9BK2 (LDHA:**21**-m) and 9BK3 (LDHA:**21**-o).

# **CRediT authorship contribution statement**

Horrick Sharma: Writing — review & editing, Writing — original draft, Visualization, Validation, Supervision, Project administration, Methodology, Investigation, Formal analysis, Conceptualization. Somrita Mondal: Investigation. Uzziah Urquiza: Investigation. Colter Esparza: Investigation. Seth Bartlett: Investigation. Landon Santa- Pinter: Investigation. Hanna Hill: Investigation. Madalyn White: Investigation. Pragya Sharma: Writing — review & editing, Supervision, Investigation, Formal analysis. Lerin Luckett-Chastain: Investigation, Formal analysis. Anne Cooper: Writing — review & editing, Investigation, Formal analysis. Mohammad Rasel: Writing — original draft, Visualization, Investigation, Formal analysis. Surendra K. Shukla: Investigation, Formal analysis. Surendra K. Shukla: Investigation, Formal analysis. Scott Lovell: Writing — review & editing, Writing — original draft, Visualization, Supervision, Investigation, Formal analysis. Michael A. Ihnat: Writing — review & editing, Visualization, Formal analysis.

# **Declaration of competing interest**

On behalf of all the authors, the corresponding author declares that there is no known financial interests or personal relationships that that could inappropriately influence (bias) the work reported in the manuscript. **Data availability** 

All data has been included in this submission

# Acknowledgements

This research is supported by financial support awarded by the National Institute of General Medical Sciences of the National Institutes of Health under OK-INBRE award number P20GM103447 subaward to Horrick Sharma. The crystallization study used resources the NYX beamline 19-ID, supported by the New York Structural Biology Center, at the National Synchrotron Light Source II, a U.S. Department of Energy (DOE) Office of Science User Facility operated for the DOE Office of Science by Brookhaven National Laboratory under Contract No. DE- SC0012704. The NYX detector instrumentation was supported by grant S100D030394 through the Office of the Director of the National Institutes of Health.

# Appendix A. Supplementary data

Supplementary data to this article can be found online at https://doi.org/10.1016/j.ejmech.2024.116598. Abbreviations

LDHA Lactate dehydrogenase-A

PDAC pancreatic ductal adenocarcinoma

OXPHOS oxidative phosphorylation LDH

Lactate dehydrogenases TFA

trifluoroacetic acid

SPR surface plasmon resonance

PER glyco-proton efflux rate

# References

- R.J. DeBerardinis, N.S. Chandel, Fundamentals of cancer metabolism, Sci. Adv. 2 (5) (2016) e1600200, https://doi.org/10.1126/sciadv.1600200.
- [2] J. Zheng, Energy metabolism of cancer: glycolysis versus oxidative phosphorylation, Oncol. Lett. 4 (6) (2012) 1151–1157, https://doi.org/10.3892/ ol.2012.928 (review).
- P. Miao, S. Sheng, X. Sun, J. Liu, G. Huang, Lactate dehydrogenase A in cancer: a promising target for diagnosis and therapy, IUBMB Life 65 (11) (2013) 904–910, https://doi.org/10.1002/iub.1216.
- [4] M.V. Liberti, J.W. Locasale, The warburg effect: How does it benefit cancer cells? Trends Biochem. Sci. 41 (3) (2016) 211–218, doi: S0968-0004(15)00241-8 [pii].
- [5] D. Hanahan, R.A. Weinberg, Hallmarks of cancer: the next generation, Cell 144 (5) (2011) 646–674, https://doi.org/10.1016/j.cell.2011.02.013.
- [6] L. Szablewski, Glucose transporters as markers of diagnosis and prognosis in cancer diseases, Onco Rev. 16 (1) (2022) 561, https://doi.org/10.4081/oncol.2022.561.

- V. Fu, T. Moroishi, K. Guan, Glycoholics anonymous: cancer sobers up with mTORC1, Cancer Cell 29 (4) (2016) 432–434, https://doi.org/10.1016/j. ccell.2016.03.016.
- [8] M.G. Vander Heiden, L.C. Cantley, C.B. Thompson, Understanding the warburg effect: the metabolic requirements of cell proliferation, Science 324 (5930) (2009) 1029–1033, https://doi.org/10.1126/science.1160809.
- H. Ying, A.C. Kimmelman, C.A. Lyssiotis, et al., Oncogenic kras maintains pancreatic tumors through regulation of anabolic glucose metabolism, Cell 149 (3) (2012) 656–670, https://doi.org/10.1016/j.cell.2012.01.058.
- [10] J. Cui, M. Shi, D. Xie, et al., FOXM1 promotes the warburg effect and pancreatic cancer progression via transactivation of LDHA expression, Clin. Cancer Res. 20 (10) (2014) 2595–2606, https://doi.org/10.1158/1078-0432.CCR-13-2407. (Accessed 11 March 2022).
- [11] Q. Zhou, G. Deng, Z. Wang, G. Dai, Preoperative lung immune prognostic index predicts survival in patients with pancreatic cancer undergoing radical resection, Front Surg 9 (2023) 1002075, https://doi.org/10.3389/fsurg.2022.1002075.
- [12] Y. Xiao, W. Chen, Z. Xie, et al., Prognostic relevance of lactate dehydrogenase in advanced pancreatic ductal adenocarcinoma patients, BMC Cancer 17 (1) (2017) 25–28, https://doi.org/10.1186/s12885-016-3012-8.
- [13] G. Claps, S. Faouzi, V. Quidville, et al., The multiple roles of LDH in cancer, Nat. Rev. Clin. Oncol. 19 (12) (2022) 749–762, https://doi.org/10.1038/s41571-022-00686-2.
- [14] J.R. Doherty, J.L. Cleveland, Targeting lactate metabolism for cancer therapeutics, J. Clin. Invest. 123 (9) (2013) 3685–3692, doi: 69741 [pii].
- [15] R. Perez-Tomas, I. Perez-Guillen, Lactate in the tumor microenvironment: an essential molecule in cancer progression and treatment, Cancers 12 (11) (2020) 3244, https://doi.org/10.3390/cancers12113244.
- [16] K.G. de la Cruz-Lopez, L.J. Castro-Munoz, D.O. Reyes-Hernandez, A. Garcia- Carranca, J. Manzo-Merino, Lactate in the regulation of tumor microenvironment and therapeutic approaches, Front. Oncol. 9 (2019) 1143, https://doi.org/10.3389/fonc.2019.01143.
- [17] D. Czaplinska, R. Ialchina, H.B. Andersen, et al., Crosstalk between tumor acidosis, p53 and extracellular matrix regulates pancreatic cancer aggressiveness, Int. J. Cancer 152 (6) (2023) 1210–1225. https://doi.org/10.1002/iic.34367.
- [18] Y. Rong, W. Wu, X. Ni, et al., Lactate dehydrogenase A is overexpressed in pancreatic cancer and promotes the growth of pancreatic cancer cells, Tumour Biol 34 (3) (2013) 1523–1530, https://doi.org/10.1007/s13277-013-0679-1.
- [19] Y. Zhou, P. Tao, M. Wang, et al., Development of novel human lactate dehydrogenase A inhibitors: high-throughput screening, synthesis, and biological evaluations, Eur. J. Med. Chem. 177 (2019) 105–115, https://doi.org/10.1016/j.ejmech.2019.05.033. https://www.sciencedirect.com/science/article/pii/S0223 52341930443X.
- [20] S.J. Allison, J.R.P. Knight, C. Granchi, et al., Identification of LDH-A as a therapeutic target for cancer cell killing via (i) p53/NAD(H)-dependent and (ii) p53-independent pathways, Oncogenesis 3 (5) (2014) e102, https://doi.org/10.1038/oncsis.2014.16.
- [21] S. Van Wilpe, R. Koornstra, M. Den Brok, et al., Lactate dehydrogenase: a marker of diminished antitumor immunity, Oncolmmunology 9 (1) (2020) 1731942, https:// doi.org/10.1080/2162402X.2020.1731942.
- [22] D. Sharma, M. Singh, R. Rani, Role of LDH in tumor glycolysis: regulation of LDHA by small molecules for cancer therapeutics, Semin. Cancer Biol. 87 (2022) 184–195, https://doi.org/10.1016/j.semcancer.2022.11.007. https://www.scienc edirect.com/science/article/pii/S1044579X22002292.
- [23] J. Billiard, J.B. Dennison, J. Briand, et al., Quinoline 3-sulfonamides inhibit lactate dehydrogenase A and reverse aerobic glycolysis in cancer cells, Cancer Metabol. 1 (1) (2013) 19, https://doi.org/10.1186/2049-3002-1-19, 19.
- [24] A. Boudreau, H.E. Purkey, A. Hitz, et al., Metabolic plasticity underpins innate and acquired resistance to LDHA inhibition, Nat. Chem. Biol. 12 (10) (2016) 779–786, https://doi.org/10.1038/nchembio.2143.
- [25] A. Le, C.R. Cooper, A.M. Gouw, et al., Inhibition of lactate dehydrogenase A induces oxidative stress and inhibits tumor progression, Proc. Natl. Acad. Sci. U.S. A. 107 (5) (2010) 2037, https://doi.org/10.1073/pnas.0914433107.
- [26] G. Rai, D.J. Urban, B.T. Mott, et al., Pyrazole-based lactate dehydrogenase inhibitors with optimized cell activity and pharmacokinetic properties, J. Med. Chem. 63 (19) (2020) 10984–11011, https://doi.org/10.1021/acs. imedchem.0c00916.
- [27] C. Granchi, I. Paterni, R. Rani, F. Minutolo, Small-molecule inhibitors of human LDH5, Future Med. Chem. 5 (16) (2013) 1967–1991, https://doi.org/10.4155/fmc.13.151.
- [28] A. Boudreau, H.E. Purkey, A. Hitz, et al., Metabolic plasticity underpins innate and acquired resistance to LDHA inhibition, Nat. Chem. Biol. 12 (10) (2016) 779–786, https://doi.org/10.1038/nchembio.2143.
- [29] S. Lobo, Is there enough focus on lipophilicity in drug discovery? Expet Opin. Drug Discov. 15 (3) (2020) 261–263, https://doi.org/10.1080/17460441.2020.1691995.
- [30] H. Sharma, P. Sharma, U. Urquiza, L.R. Chastain, M.A. Ihnat, Exploration of a large virtual chemical space: identification of potent inhibitors of lactate dehydrogenase- A against pancreatic cancer, J. Chem. Inf. Model. 63 (3) (2023) 1028–1043, https://doi.org/10.1021/acs.jcim.2c01544.
- [31] T. Chung, E. Kim, C.W. Han, et al., Machilin A inhibits tumor growth and macrophage M2 polarization through the reduction of lactic acid, Cancers 11 (7) (2019) 963, https://doi.org/10.3390/cancers11070963, doi: 10.3390/ cancers11070963.
- [32] H.E. Purkey, K. Robarge, J. Chen, et al., Cell active hydroxylactam inhibitors of human lactate dehydrogenase with oral bioavailability in mice, ACS Med. Chem. Lett. 7 (10) (2016) 896–901, https://doi.org/10.1021/acsmedchemlett.6b00190.
- [33] J.K. Caines, D.A. Barnes, M.D. Berry, The use of seahorse XF assays to interrogate realtime energy metabolism in cancer cell lines, Methods Mol. Biol. 2508 (2022) 225–234, https://doi.org/10.1007/978-1-0716-2376-3\_17.

- [34] G.K.Y. Chan, T.L. Kleinheinz, D. Peterson, J.G. Moffat, A simple high-content cell cycle assay reveals frequent discrepancies between cell number and ATP and MTS proliferation assays, PLoS One 8 (5) (2013) e63583, https://doi.org/10.1371/journal.pone.0063583.
- [35] C.B. Westphalen, K.P. Olive, Genetically engineered mouse models of pancreatic cancer, Cancer J. 18 (6) (2012) 502–510. https://doi.org/10.1097/PPO.0b013e31827ab4c4.
- [36] N. Oshima, R. Ishida, S. Kishimoto, et al., Dynamic imaging of LDH inhibition in tumors reveals rapid in vivo metabolic rewiring and vulnerability to combination therapy, Cell Rep. 30 (6) (2020) 1798–1810.e4, https://doi.org/10.1016/j. celrep.2020.01.039.
- [37] G.M. Sheldrick, SHELXT integrated space-group and crystal-structure determination, Acta Crystallogr A Found Adv 71 (Pt 1) (2015) 3–8, https://doi. org/10.1107/\$2053273314026370.
- [38] G.M. Sheldrick, Crystal structure refinement with SHELXL, Acta Crystallogr C Struct Chem. 71 (Pt 1) (2015) 3–8, https://doi.org/10.1107/S2053229614024218.
- [39] J. Hu, H. Qin, F.P. Gao, T.A. Cross, A systematic assessment of mature MBP in membrane protein production: overexpression, membrane targeting and purification, Protein Expr. Purif. 80 (1) (2011) 34–40, https://doi.org/10.1016/j.pep.2011.06.001.
- [40] W. Kabsch, Xds, Acta Crystallogr D Biol Crystallogr 66 (Pt 2) (2010) 125–132, https://doi.org/10.1107/S0907444909047337.
- [41] C. Vonrhein, C. Flensburg, P. Keller, et al., Data processing and analysis with the autoPROC toolbox, Acta Crystallogr D Biol Crystallogr 67 (Pt 4) (2011) 293–302, https://doi.org/10.1107/S0907444911007773.
- [42] P.R. Evans, An introduction to data reduction: space-group determination, scaling and intensity statistics, Acta Crystallogr D Biol Crystallogr 67 (Pt 4) (2011) 282–292, https://doi.org/10.1107/S090744491003982X.
- [43] A.J. McCoy, R.W. Grosse-Kunstleve, P.D. Adams, M.D. Winn, L.C. Storoni, R. J. Read, Phaser crystallographic software, J. Appl. Crystallogr. 40 (Pt 4) (2007) 658–674, https://doi.org/10.1107/S0021889807021206.
- [44] P.D. Adams, P.V. Afonine, G. Bunkoczi, et al., PHENIX: a comprehensive python-based system for macromolecular structure solution, Acta Crystallogr D Biol Crystallogr 66 (Pt 2) (2010) 213–221, https://doi.org/10.1107/S0907444909052925.
- [45] P. Emsley, B. Lohkamp, W.G. Scott, K. Cowtan, Features and development of coot, Acta Crystallogr D Biol Crystallogr 66 (Pt 4) (2010) 486–501, https://doi.org/ 10.1107/S0907444910007493.
- [46] V.B. Chen, W.B.3 Arendall, J.J. Headd, et al., MolProbity: all-atom structure validation for macromolecular crystallography, Acta Crystallogr D Biol Crystallogr 66 (Pt 1) (2010) 12– 21. https://doi.org/10.1107/S0907444909042073.
- [47] L. Potterton, S. McNicholas, E. Krissinel, et al., Developments in the CCP4 molecular-graphics project, Acta Crystallogr D Biol Crystallogr 60 (Pt 12 Pt 1) (2004) 2288–2294, https://doi.org/10.1107/S0907444904023716.
- [48] E. Krissinel, Enhanced fold recognition using efficient short fragment clustering, J. Mol. Biochem. 1 (2) (2012) 76–85.
- [49] M.D. Winn, C.C. Ballard, K.D. Cowtan, et al., Overview of the CCP4 suite and current developments, Acta Crystallogr D Biol Crystallogr 67 (Pt 4) (2011) 235–242, https://doi.org/10.1107/S0907444910045749.
- [50] D. Liebschner, P.V. Afonine, N.W. Moriarty, et al., Polder maps: improving OMIT maps by excluding bulk solvent, Acta Crystallogr D Struct Biol 73 (Pt 2) (2017) 148–157, https://doi.org/10.1107/S2059798316018210.